Canadian Science Publishing | Canadian Geotechnical Journal

Smart Determination of Borehole Number and Locations for Stability Analysis of Multi-layered Slopes using Multiple Point Statistics and Information Entropy

Journal:	*Canadian Geotechnical Journal*
Manuscript ID	cgj-2020-0327.R2
Manuscript Type:	Article
Date Submitted by the Author:	02-Dec-2020
Complete List of Authors:	Shi, Chao; City University of Hong Kong, Department of Architecture and Civil Engineering Wang, Yu; City University of Hong Kong, Dept of Civil and Architectural Engineering
Keyword:	multiple point statistics, slope stratigraphy, sparse measurements, information entropy, data-driven model
Is the invited manuscript for consideration in a Special Issue? :	Not applicable (regular submission)

Smart Determination of Borehole Number and Locations for Stability Analysis of Multi-layered Slopes using Multiple Point Statistics and Information Entropy

Chao Shi [a] and Yu Wang [b]*

[a] Department of Architecture and Civil Engineering, City University of Hong Kong, Tat Chee Avenue, Kowloon, Hong Kong, China. (Email): chaoshi6-c@my.cityu.edu.hk

[b] Department of Architecture and Civil Engineering, City University of Hong Kong, Tat Chee Avenue, Kowloon, Hong Kong, China. (Email): yuwang@cityu.edu.hk (**Corresponding author**)

Abstract

Subsurface stratigraphy of multi-layered slopes is essential and crucial for slope stability analysis. It is usual practice for engineers to interpret stratigraphic boundaries separating different soil layers using both site investigation data and prior knowledge of local geology, but such practice might encounter significant challenge when the site data are very limited. In addition, uncertainty in stratigraphic boundaries has not been explicitly or quantitatively considered in planning of site investigation (e.g., determination of borehole number and locations). There lacks a quantitative and objective tool to determine the optimal locations and number of boreholes for slope stability analysis while accounting for stratigraphic uncertainty. In this study, a smart sampling strategy based on multiple point statistics and information entropy is proposed for delineation of slope subsurface stratigraphy and planning of geotechnical boreholes. It is a data-driven approach that enables an ensemble of prior knowledge within a training image using multiple point statistics. The proposed method not only provides evolution of the most probable interpolation from sparse measurements and the associated interpolation uncertainties, but also adaptively determines the optimal locations of boreholes. Effectiveness of the proposed method is illustrated and validated through both a simulation example and a real case. It is found that the data-driven framework can automatically identify location of largest interpolation uncertainty within a multi-layered slope conditional on its outcrops, and that the associated stratigraphic uncertainty gradually reduces as borehole number increases. More importantly, the optimal number and locations of boreholes required for slope stability analysis is adaptively determined by the proposed method.

Keywords: multiple point statistics; slope stratigraphy; sparse measurements; information entropy; data-driven model

1. Introduction

An accurate geotechnical site characterization is essential and crucial for evaluation of slope stability. It is well acknowledged that slope stability can be significantly affected by soil heterogeneities, particularly multiple soil strata within a slope and the uncertainty associated with stratigraphic boundaries (Bossi et al. 2019; Elkateb et al. 2003; Hansen et al. 2007). The stratigraphic uncertainty is referred to the uncertainty of boundaries or interfaces separating different soil strata and frequently reflected as interbedded layers or inclusion of soil pockets within a relatively uniform soil mass (e.g., Gong et al. 2019; Liu et al. 2017b; Liu et al. 2020; Wang et al. 2018a). Stratigraphic uncertainty is considered a dominating source of uncertainty for stability of multiple-layered slopes as geotechnical properties are often quite different in different strata (e.g., Phoon 2017; Wang et al 2018). Therefore, an accurate delineation and characterization of soil stratigraphic boundaries play a central role in slope stability assessment (Juang et al. 2019; L'Heureux et al. 2012; Wang et al. 2019).

Delineation of subsurface stratigraphy of multi-layered slopes is challenging particularly when site-specific measurements (e.g., boreholes) are sparse and limited. Consider, for example, a real multiple-layered slope in Hong Kong as illustrated in Fig. 1. Outcrops along the pre-cut slope surface reveal that there are three different soil layers, namely, colluvium (Col), residual soil (RS) and completely decomposed granite (CDG). When delineating extents of stratigraphic boundaries between different strata based on available outcrops, as a first approximation, it may be feasible to describe stratigraphic dips of colluvium and residual soils by assuming soil strata in parallel to slope surface. However, it is impossible to determine the thickness and boundaries of CDG solely based on the geological information revealed from the exposed outcrops as no relevant spatial geological information is available. Even if one borehole is allowed for investigating the

subsurface stratigraphy, spatial distributions of the highly decomposed granite (HDG) and moderately decomposed granite (MDG) still cannot be determined from the known stratigraphy provided by the additional borehole.

The dilemma in the above example cannot be resolved by usual engineering practice, which interprets subsurface stratigraphy by drawing straight lines to connect deterministic stratum boundary at adjacent measurements (e.g., boreholes). Although this usual practice is acceptable for slopes with simple geology or extensive measurements, for multi-layered slopes with outcrops only or one borehole (e.g., the example in Fig.1), the delineation of subsurface stratigraphy is an impossible task. In addition, the stratigraphic uncertainty and risk in the above example can hardly be mitigated even with more advanced probabilistic methods, such as Coupled Markov Chain (CMC) method (Elfeki and Dekking 2001; Li et al. 2016; Liu et al. 2020; Qi et al. 2016) and Markov Random Field (MRF) method (Gong et al. 2019; Li et al. 2016; Wang 2020; Wang et al. 2018; Wang 2019). The successful application of CMC requires an accurate estimation of stationary transition probability in both horizontal and vertical directions, but such probability cannot be evaluated properly if only slope outcrop or one borehole is available. For MRF, stratigraphic dip and spatial anisotropy of stratigraphic boundaries should be explicitly defined via local configuration template for delineation of subsurface stratigraphy. A reliable specification of local lithological distribution normally requires prior knowledge and understanding of the local geology, which poses a difficulty in practical application (e.g., the slope example in Fig. 1) as measurements are limited in quantity.

Another difficulty in geotechnical site characterization in the above example is the determination of adequate number and optimal locations of boreholes for slope stratigraphy. For engineering practice, borehole sampling plan is normally made based on standard procedures outlined in codes

and guidelines (e.g., GCO 2017), which specify uniformly spaced boreholes without accounting for subsurface stratigraphic uncertainty. This existing planning practice does not make full use of prior knowledge to reduce geological uncertainties and can possibly result in an inefficient site investigation plan. The situation gets even worse for slopes, whose site-specific stratigraphy is normally interpreted from sparse measurements (e.g., one or two boreholes). How to determine the optimal locations and number of boreholes for reliable evaluation of slope stability remains an unsolved problem. There lacks a rational way to determine the value associated with each borehole for reliable slope subsurface stratigraphy and stability analysis.

The slope example in Fig. 1 underscores the necessity of an objective and quantitative method to determine the optimal number and locations of boreholes, often limited, for slope stability analysis. This study aims to develop a smart strategy to adaptively interpolate subsurface stratigraphy from sparse measurements and to implement a data-driven procedure for planning of borehole layout. The proposed method is based on multiple point statistics (MPS) and enables incorporation of all valuable prior knowledge, e.g., pre-existing engineering experience from previous projects at nearby sites or with similar geological settings, into a single training image for stochastic simulation. This effectively combats the intrinsic difficulty associated with sparse measurements in geotechnical site investigation. It is a data-driven method that not only estimates the most probable interpolation from sparse measurements but also actively identifies zones with largest interpolation uncertainties, which further facilitates an adaptive process for determining the optimal borehole locations and number based on the principle of maximum entropy reduction. Effects of stratigraphic uncertainty on the slope stability analysis results are also explicitly investigated. The proposed non-parametric and data-driven strategy can easily be implemented and is illustrated via both simulation example and real slope case.

The reminder of this study is organized as follows. In the second section, a smart sampling strategy is proposed for determining the optimal number and locations of limited boreholes for stability analysis of slopes considering stratigraphic uncertainty. Spatial interpolation of subsurface stratigraphy of multi-layered slopes from limited measurements (e.g., outcrops and boreholes) by MPS and quantification of interpolation uncertainty based on information entropy are explained. In the third section, detailed implementation procedures are discussed. Subsequently, a heterogeneous slope profile is simulated to illustrate performance of the proposed method. Effects of different MPS training images on slope stability analysis are also explicitly investigated. Finally, real geological profiles from a slope in Hong Kong are used to further demonstrate performance of the proposed method.

2. Proposed adaptive sampling strategy for stability analysis of multi-layered slopes

Fig. 2 illustrates the proposed data-driven framework for determining optimal locations and number of boreholes for subsurface stratigraphy of multi-layered slopes. The investigation process starts with desk study and site reconnaissance (e.g., Clayton et al. 1995; GCO 2017; Wang et al. 2016), during which prior knowledge (e.g., geological maps, published reports and studies) are integrated with engineer judgement for planning of site investigation. Slightly different from general site characterization procedures summarized by Wang et al. (2016), there is no direct linkage between site reconnaissance and in-situ borehole investigation. All the available prior knowledge is collected and concisely represented into a training image, which combines with site-specific outcrops to perform MPS stochastic simulation for slope stratigraphy. The quality and performance of the stochastic simulation are regulated via slope stability analysis results using

preliminary estimate of soil properties from borehole observation (e.g., SPT-N data). As the number of site-specific boreholes increases, the stochastic simulation becomes increasingly constrained and the subsurface stratigraphy gradually converges to the true subsurface condition, leading to an improved FoS estimate. The overall sampling plan is updated and new boreholes are carried out if there is a large variation in the calculated slope stability results. Subsequently, the retrieved geotechnical information (e.g., soil type) from additional borehole is combined with outcrops and training image to update MPS stochastic simulation. The whole updating process continues until slope stability analysis results converge. In the following subsections, key elements of the proposed smart sampling strategy are described with details.

2.1 Ensemble prior knowledge in training image

All valuable prior knowledge (e.g., soil survey maps and geological maps) are collected and concisely represented in a single conceptual training image. The use of an ensemble training image overcomes the difficulty of casual geological interpretation procedure, which combines piecewise prior knowledge and engineering judgement for spatial interpolation, and provides a handy tool to incorporate all the prior stratigraphic information (e.g., dip and stratigraphic connectivity) in a single geological model in a quantitative and objective manner. It should be noted that the training image does not require to be accurate but should enclose all stratigraphic relationships, which are believed to be representative of local geology in the location of interest. It is beneficial if the spatial structures are homogeneously distributed within a training image (Mariethoz and Caers 2014; Strebelle and Remy 2005). In geoscience community where MPS is widely used, a training image can be constructed from process-based models, process-mimicking models and unconditional

object-based simulation (Mariethoz and Caers 2014). In geotechnical site characterization, as interpreted geological profiles are available for each finished geotechnical project, there is a rich database of training images from previous projects. Therefore, for geotechnical application (e.g., slope subsurface stratigraphy), training image can be directly obtained from previous geotechnical projects at nearby sites or with similar geological settings, e.g., simply a geological profile borrowed from an interpreted geological cross section in close proximity (e.g., Shi and Wang 2020b) or even a hand-drawn conceptual geological model for a given geological setting (e.g., Fadlelmula et al. 2016; Tahmasebi 2018). The compatibility between a training image and site-specific measurements can be evaluated based on the spatial stratigraphic patterns derived from the training image and site-specific measurements. Boisvert et al. (2007) proposed to rank compatibility of a training image with conditioning data through comparison of distribution of runs (Mood 1940) and multiple-point density function (MPDF) of vertical one-dimensional boreholes. Further studies are required on this aspect but beyond the scope of this study. There is great potential for combing training image concept with markov-based models, e.g., Coupled Markov Chain and Markov Random Field (e.g., Gong et al. 2020; Wang 2020), for solving practical geotechnical problems. The application of training image is most valuable for slope projects as measurements (e.g., outcrops and one or two boreholes) are normally limited in quantity.

2.2 Stochastic stratigraphic modelling for slope stratigraphy using multiple point statistics

The stochastic simulation of slope stratigraphy in the proposed data-driven framework (refer to Fig.2) is performed using MPS, which is a non-parametric stochastic simulation tool for interpolation of stratigraphic boundaries. MPS was first proposed by Guardiano and Srivastava

(1993) to replicate complex spatial connectivity among different geo-bodies. It extends the concept of indicator kriging, which relies on two-point statistics for simulating geological structures, and employs higher-order statistics, e.g., trivariate and quadrivariate, for stochastic simulation. It is worthwhile to mention that MPS does not rely on any pre-determined parametric function form for deducing subsurface stratigraphy and directly infers soil types at un-sampled locations from a conceptual training image. The direct application of previous geological cross-sections for training is based on the assumption of similar local spatial connectivity or stratigraphic relationships between soils in areas with similar geological settings. MPS has been successfully applied in various disciplines, e.g., hydrogeology and geological engineering (Mariethoz and Renard 2010; Shi and Wang 2020a). Recently, Shi and Wang (2020b) adopted MPS to delineate subsurface geological profiles of a real reclamation project in Hong Kong. MPS is particularly beneficial for slope stratigraphy in practice, which involves significant uncertainty in the interpretation of subsurface stratification from limited outcrops and borehole data.

Fig. 3 illustrates key steps for running MPS simulation. Detailed description is referred to Shi and Wang (2020b). Soil type of the blank cell with a question mark in the simulation image is inferred by sampling similar spatial features from an ensemble training image while conditioning on available measurements (e.g., outcrops and borehole data). Outcrops along slope surface essentially provide a continuous line measurement reflecting important stratigraphic relationships of subsurface strata, and they may be leveraged on during slope stratigraphy. The stratigraphic pattern searching process relies on data event template, which is defined as several closest measurements around a target point without direct measurement. The data event template in Fig.3 is circled by dashed line and consists of three conditional cells, i.e., yellow, green and blue cells, representing available measurements. The same data event template is used to scan the training

image to find all the replicate data events. A qualified data event within the training image is found when all of its surrounding conditional cells are identical to those of the data event template in the test image, i.e., with the same number and color. For example, the three conditional cells of example 1 in the training image fulfils above conditions and the associated difference is 0. In comparison, the bottom two conditional cells of example 2 have different colors from the data event template and account for 2/3 of all three conditional cells. Therefore, associated event distance between example 2 and the search data event template is 2/3. After collecting all the qualified training data events, a random sample is drawn from the collection and pasted to the central unknown cell (i.e., the cell with a question mark) in the simulation image. Following a random simulation path, all the un-sampled cells can be inferred one by one and a realization is completed.

Repeating the above stochastic simulation procedures, multiple realizations conditioning on the same set of measurement data and training image are generated. Afterwards, the most probable slope profile can be estimated by statistical analysis of multiple realizations. The associated interpolation uncertainties can also be explicitly quantified and analyzed based on information entropy. More details about uncertainty quantification are discussed in section 2.3. To evaluate performance of stochastic simulation in the simulated examples in the following sections, where the underlying true test image is completely known, prediction accuracy, denoted as *Acc*, is employed to measure the deviation of most probable interpolation from the underlying true test image.

$$Acc = \frac{\sum_{i=1}^{N_h \times N_v} \boldsymbol{I}\left(Z_T(x_i) = Z_{mp}(x_i)\right)}{N_h \times N_v} \quad (1)$$

where N_h and N_v denote the horizontal and vertical size of a simulation grid; $Z_T(x_i)$ is soil type at location x_i within a test image; $Z_{mp}(x_i)$ is the most probable interpolation, which represents the soil type with highest occurrence frequency at location x_i; $I(\cdot)$ is an indicator function that takes the value of one when the soil type in test image, i.e., $Z_T(x_i)$, is identical to that in the most probable interpolation $Z_{mp}(x_i)$, and otherwise, has the value of zero. Eq. (1) can also be used to evaluate similarity between two realizations by simply replacing $Z_T(x_i)$ and $Z_T(x_i)$ with those of corresponding realizations. It should be clarified that in practical geotechnical engineering, the true test image for the location of interest is unavailable. Eq. (1) is used here only to illustrate the validation of the stochastic stratigraphic simulation method.

2.3 Adaptive determination of optimal borehole locations using information entropy

An optimal sampling location should be selected in order to retrieve as much subsurface geological information as possible and simultaneously reduce potential interpolation uncertainty. Such uncertainty can be quantified and analyzed by information entropy, which provides a unified measure for uncertainty quantification without assumptions of any parametric function forms or evaluation of any statistics (e.g., mean and variance) (e.g., Wellmann 2013). Information entropy was first proposed by Shannon (1948) to identify the amount of information required to transmit signals in electronic engineering and signal processing. The term "entropy" denotes disorder or unpredictability of a random variable at a single position, and can be integrated to reflect average information associated with a random field or process. A key significance for information entropy is to facilitate a direct representation of 'amount of uncertainty' by a scalar measure (Jaynes 2003). An increase in information entropy is equivalent to an increase in complexity or unpredictability

of a random process (Batty et al. 2014), and vice visa. Specifically, information entropy, i.e., H, is zero if a random variable Z possesses no uncertainty with occurrence probability $p(Z)$ equals to zero or one. Mathematically, information entropy H at each spatial location x can be calculated by the following formulation.

$$H(x) = -\sum_i^N \{p_i[Z\,(x)] \cdot lnp_i[Z(x)]\} \quad (2)$$

where $p_i[Z(x)]$ refers to the occurrence probability of each possible outcome i out of N possible outcomes. The minimum value of H is zero, denoting no uncertainty. On the other hand, a maximum value is obtained when N possible outcomes are equally likely, i.e., $p_i[Z(x)] = 1/N$. For subsurface stratigraphic interpolation, information entropy can be used as a quantitative measure of geological uncertainty at each location in space, allowing a direct comparison of interpolation uncertainty. It has been successfully applied to geological modelling (e.g., Wang 2018; Wellmann and Caumon 2018; Wellmann and Regenauer-Lieb 2012) and geotechnical site characterization (Wang et al. 2013; Zhao and Wang 2019).

For slope subsurface stratigraphy, a slope domain (i.e., a 2D vertical cross-section) can be discretized into a grid and soil category at each grid point is considered a random variable. Uncertainty of soil types at each point can be concisely quantified by information entropy, which serves a simple tool in evaluating and visualizing performance of spatial interpolation in model space. The calculated information entropy at every point is collected and shown as a single entropy map. It is worth noting that if actual measurement has been taken at a point, the corresponding entropy value diminishes to zero, because of the known soil type at the measured point. From the constructed entropy map, it is easy to identify zones with the largest interpolation uncertainty, and the optimal location for the next borehole can be determined in accordance with the principle of

maximal entropy reduction. Since borehole is often conducted vertically, it is beneficial to sum up entropy values along each vertical 1D line for easy comparison of stratigraphic uncertainty at any potential borehole location (i.e., any horizontal distance within the 2D vertical cross-section). In this way, 2D vertical entropy map can be converted into a 1D entropy curve varying along horizontal distance, and total entropy values along a vertical line profile at a given horizontal distance is represented by a point in the entropy curve.

Entropy map and entropy curve of slope can be sequentially updated with the addition of new boreholes. Based on the variation of entropy curve, an adaptive sampling procedure can be implemented (refer to Fig. 2). At the beginning of slope stratigraphy, only outcrops serve as conditioning information (i.e., measurement data) for constraining stochastic simulation, resulting in large interpolation uncertainties. The calculated total information entropy at an arbitrary horizontal location x_h can be expressed as $H(x_h,0)$, where "0" stands for zero borehole. When one additional borehole (i.e., line measurement) is added, the updated entropy, i.e., $H(x_h,1)$, around the added borehole reduces. With an increase in number of boreholes, there is a sequential reduction in estimated entropy values in space. Mathematically, total entropy at any horizontal distance x_h is represented as $H(x_h,n_b)$, where n_b denotes the total number of boreholes. The reduction in the total entropy, i.e., Δ_{n_b} at x_h during sequential updating process can be formulated as follows.

$$\Delta_{n_b} = H(x_h,n_b - 1) - H(x_h,n_b),\ n_b = 1, 2, 3... \quad (3)$$

The magnitude of Δ_{n_b} represents the additional stratigraphic information associated with the n_b-th borehole and reflects the value of each additional borehole. A large Δ_{n_b} is equivalent to a large

reduction in stratigraphic uncertainty. Therefore, determination of the optimal borehole location reduces to an optimization problem of finding the maximal Δ_{n_b}.

2.4 Determination of borehole number based on slope stability analysis results

The most probable interpolation of slope profile obtained from MPS scholastic simulation gradually approaches to the underlying true profile as the number of boreholes increases. There exists a trade-off between borehole number and spatial interpolation performance. Therefore, when to stop adding borehole depends on effects of stratigraphic uncertainties on overall stability of the slope. A commonly-used performance indicator in slope stability analysis is Factor of Safety (FoS). At a given number of borehole, each realization from MPS stochastic simulation may be used to perform slope stability analysis, leading to a FoS value. When only limited measurements are available, there is a large stratigraphic uncertainty, resulting in a large variation in the calculated FoS from multiple realizations. As the incorporation of more boreholes, the stratigraphic boundaries get more constrained, and the associated interpolation uncertainties with multiple realizations get significantly reduced, leading to a stabilized FoS trend. The termination criterion of adding additional boreholes depends on budget and risk acceptance level, e.g., probability of failure or reliability index. For example, when the mean FoS calculated from multiple realizations is higher than a pre-specified FoS, e.g., 2.0, no further borehole is required as borehole drilling is an expensive operation. Generally speaking, when the FoS approaches a constant (e.g., the percentage change in mean values of FoS (i.e., μ_{FoS}) is less than a small threshold, say 1%), the data-driven sampling procedure can be terminated, and no additional borehole is needed.

3. Implementation procedure

Fig. 4 illustrates key procedures of the proposed smart sampling strategy for stratigraphy and stability analysis of slopes. Seven steps are involved in the proposed method, as summarized below.

1. Discretize slope domain into a grid size of $N_h \times N_v$ with corresponding resolutions of λ_h and λ_v along horizontal and vertical direction, respectively.

2. Collect all the prior stratigraphic information (e.g., geological profile from previous projects at nearby sites or with similar geological setting) of the simulation grid and concisely present it in a single training image.

3. Run multiple MPS stochastic simulations conditioning on outcrops and other measurements (e.g., borehole), if any, until the change in the most probable interpolation is negligible (e.g., less than 0.1%).

4. Evaluate overall slope stability of multiple realizations generated in step 3.

5. Check if the mean of calculated FoS is larger than a pre-specified value such as 2.0. If yes, no slope design is required.

6. Statistical analysis of the FoS obtained from all the realizations to check if percentage change in the mean of FoS, i.e., μ_{FoS}, is less than 1%. If larger than 1%, evaluate the total information entropy $H(x_h, n_b)$ along horizontal direction, and specify the next borehole location based on the maximum reduction in entropy Δ_{n_b}.

6. Repeat steps 3 to 5 until stratigraphic uncertainty diminishes with percentage change in μ_{FoS} is less than 1%.

7. Delineate slope stratigraphy for slope design.

Although procedures for the proposed smart sampling strategy involve seven steps, they can be easily implemented using software, such as Python 3.7 and commercial slope stability analysis software such as FLAC or Slope/W.

4. Illustrative example

In this section, the proposed method is illustrated using a simulated slope example. The process of generating training and test images of slope stratigraphy are described. A typical slope profile consisting of four different soil types is simulated, as shown in Fig. 5a and 5b. The total horizontal length and vertical height are 30m and 15m, respectively. The bi-directional resolution is 0.1m, resulting in a total of 45000 points. The resolution is determined based on mesh size commonly adopted in numerical modelling of geotechnical analysis, e.g., about 0.1m – 1.0m for finite element/difference modelling of foundation, deep excavation, or slope stability analysis (e.g., Ching and Hu 2016; Liu and Deng 2019; Wang et al. 2016; Sazzad et al. 2015) or conventional sampling interval used in geotechnical site investigation, e.g., a sampling interval of about 1m for standard penetration tests (e.g., Kulhawy and Mayne 1990). Both outcrops and stratigraphic boundaries separating different soil layers are delineated by five quadratic lines (i.e., I, II, III, IV and V in Fig. 5b).

$$d = a \times h^2 + b \times h + c \quad (4)$$

where h and d refer to the horizontal distance and elevation along slope; a, b and c are coefficients of each quadric line and taken to follow Gaussian distributions. The mean and standard deviation of each coefficient are listed in Table 1.

Fig. 5a and Fig. 5b show the generated test and training images following Eq. (4). Both images share similar geological settings with a calculated similarity of 68.6% based on Eq. (1). The training image serves as the graphic representation of ensemble prior knowledge for the test image. It is clear that soil1 in training image is more uniform in total thickness with stratigraphic boundaries lying almost parallel to outcrops. In comparison, soil1 in the test image is much thinner and non-uniform in total thickness. It should be noted that only outcrops along the slope surface of test image are taken as measurements for interpretation of slope stratigraphy at the beginning of the proposed smart sampling method. In addition, three different training images are generated in order to investigate effects of MPS training images on slope stability analysis. The training images in Fig. 5c and 5d, i.e., TI1 and TI2, are generated by scaling and flipping the original training image, i.e., TI0, in Fig. 5b. The scaled training image in Fig. 5c approximately reduces the thickness of soil2 and soil3 layers by half. In comparison, the flipped training image in Fig. 5d transforms convex and concave stratigraphic boundaries into their counterparts, i.e., concave and convex. Based on Eq. (1), the similarity of scaled and flipped training images with respect to the test image is calculated as 43.1% and 70.2%, respectively. The similarity of two images is calculated by a ratio between the number of cells that have the same soil type and spatial coordinates over the total number of cells in the image. Two identical images are considered to have a similarity of 1. Moreover, a fourth training image, i.e., TI3, in Fig. 5e with a relatively gentle slope is generated following Eq. (4), and its similarity with respect to the test image is 92.8%.

5. Results obtained from the proposed method

Following the procedures described in the previous sections, multiple realizations from stochastic simulation conditioning on outcrops are generated. All the control parameters for performing MPS simulation are summarized in Table 2. The key input parameters required for running stochastic simulation is the maximum number of conditioning point within a data event n and acceptable threshold t for distance measure. The detailed interpretation and specification of both parameters are discussed by Shi and Wang (2020b). The number of realizations is determined when the percentage change in the most probable interpolation is less than 0.1% for every 10 additional realizations. Fig. 6a shows the evolution of the most probable interpolation. It is clear that there is an overall reduction trend of the percentage change in most probable interpolation as the realization number increases. The percentage change decreases to less than 0.10% when the total number of realizations is over 80. Consequently, 100 realizations are generated in this study. Similar results are also shown in Fig. 6b. The accuracy of each soil layer for the most probable interpolation stabilizes after 20 stochastic simulations. Note that the accuracy measure is used for validation purpose here and is not available in engineering practice because the true site stratigraphy is unknown.

5.1 Most probable interpolation with quantified uncertainty

The most probable interpolation from 100 realizations is shown in Fig. 7a. It is clear that the spatial connectivity of different strata can be reasonably captured with an overall prediction accuracy of about 74.5% even though no borehole samples are retrieved from the site. As soil types along slope outcrops are actual measurements, soil layers close to those outcrops are correctly replicated. More

importantly, the overall stratigraphic boundaries of soil4 can be approximately delineated from stochastic simulation even though no samples of soil4 are available. When compared with the true test image in Fig. 5a, it is observed that the largest deviations lie in the stratigraphic boundaries between soil1 and soil2. This can be attributed to the fact that soil layers away from outcrops are not constrained by measurements and simply replicating spatial patterns in the training image.

Stratigraphic uncertainty at each point within the model space is calculated by information entropy defined in Eq. (2). All the point entropy values are collected and shown as an entropy map in Fig. 7b. It is clear that bands of large entropy values cluster around stratigraphic boundaries separating different soil layers, indicating large interpolation uncertainties associated with interpreted soil boundaries. For points away from stratum boundaries, entropy values gradually diminishes to zero. It is conceivable that as the incorporation of more borehole measurements, extents of zones with large entropy values can significantly shrink. For easy determination of the optimal sampling location, total entropy along horizontal distance of the slope is plotted in Fig. 7c. Evidently, as the horizontal distance from slope toe increases from 5 to 16.8m, the total entropy increases monotonically to a peak of about 35, and it gradually reduces to about 10 when the distance further increases beyond 16.8m. Based on Eq. (3), the maximum entropy reduction Δ_1 (i.e., $H(x_h,0) - H(x_h,1)$ is achieved where $H(x_h,0)$ has the maximum value because $H(x_h,1)$ becomes zero when borehole is performed at this location (i.e., measurements are taken at location (i.e., x_h)). Consequently, the next borehole probe should be carried out at 16.8m away from slope toe.

Each slope profile obtained from stochastic simulation is adopted for slope stability analysis (e.g., using FLAC). The soil parameters of each soil layer are summarized in Table 3. Fig. 8a shows the model setup of one realization. The slope is modelled by quadrilateral element with a size of 0.2m × 0.2m. According to the manual of FLAC7.0 (Itasca 2013; 2014), quadrilateral element is the

smallest geometric domain used in FLAC, and each element is internally divided into four triangular "subzones". The FoS in FLAC is calculated using strength reduction method. The resulted maximum shear strain rate upon failure is shown in Fig. 8b. The calculated FoS is 1.20, and the resulted slip surface mainly passes through soil1 and soil3. It is conceivable that any changes in the stratigraphic extent of those soils may affect the slip surface. In addition, calculated FoS for all 100 realizations are shown in Fig.8c. Obviously, the overall FoS mainly fluctuates between 1.14 and 1.26 with a mean (μ) and standard deviation (σ) of 1.202 and 0.024, respectively. Much finer element size, i.e., 0.1m, is also adopted to check the robustness of stability analysis, and similar FoS results are obtained. For computational efficiency, the element size is taken as 0.2m.

5.2 Smart determination of optimal locations and number of boreholes

Sequential updating of slope stratigraphy as the inclusion of more borehole measurements is shown in Fig. 9. According to the total entropy curve in Fig. 7c, the next borehole should be carried out at a horizontal distance of 16.8m. Conditioning on the outcrops and additional borehole (i.e., the soil type along a vertical line at the horizontal distance of 16.8 m in the test image, Fig. 5a, is taken as the borehole data), another 100 realizations are generated with a percentage change in most probable interpolation less than 0.10%. Fig. 9a shows the corresponding most probable interpolation. Evidently, the most probable interpolation, particularly soil1 and soil2, becomes more resemble to the true test image in Fig. 5a with an accuracy of 85.0%. This can be explained by the fact that spatial distribution of soils around the newly added borehole get more constrained during multiple stochastic simulation. The change in the most probable interpolation can be better

reflected in the entropy map in Fig.9b. Different from the prominent continuous entropy band as shown in Fig.7b, zones of large entropy values shrink significantly, particularly at location of the borehole. Similarly, entropy values at close proximity to the borehole significantly decrease, reflecting the improvement in spatial interpolation of subsurface stratigraphy. When examining the total entropy along the horizontal distance in Fig.9c, the original peak total entropy shown in Fig.7c disappears and is replaced by a new, but relatively small peak at 19.7m away from slope toe.

Following simulation procedures illustrated in the flowchart in Fig. 4, the optimal sampling location for subsequent stratigraphy updating can be obtained by consecutively examining location of maximum entropy. Based on total entropy plot in Fig. 9c, the next optimal sampling locations are determined to be at 19.7m from slope toe. The updated most probable interpolation from additional 100 stochastic realizations are shown in Fig. 9d. The corresponding accuracy increases to 88.2%. Similarly, the results associated with the addition of the 3rd borehole are shown in Figs. 9f&g, and the accuracy further improves to 93.5%. With the addition of 2nd and 3rd borehole, extents of soil1 and soil2 reduces and increases, respectively, and become more similar to the true stratigraphic boundaries shown in Fig. 5a. Simultaneously, there is a significant reduction in entropy at zones around added boreholes, and peak values of total entropy curves in Figs. 9f and 8i along horizontal direction continue to reduce. It should be noted that in practical geotechnical site characterization, the true test image is not available, and the accuracy cannot be calculated. Therefore, the entropy map may also be treated as an indicator of interpolation quality.

Evolution of FoS for stochastic simulation conditional on different numbers of boreholes is shown in Fig. 10a. When borehole number increases from zero to three, the mean values of FoS monotonically decrease from 1.202 to 1.140 with corresponding standard deviation reduces from

0.024 to 0.014. For comparison, the FoS of 1.140 calculated from the true test slope profile in Fig. 5a is also shown in the figure. There is a tendency of calculated FoS towards the true FoS as the incorporation of more boreholes. This makes sense as stochastic simulation gets better constrained by more measurements, leading to a reduction in standard deviation of FoS. The histograms of FoS for different borehole numbers are shown in Fig. 10b. There is a consistent reduction in the mean (μ) and standard deviation (σ) of the calculated FoS with an increasing borehole number. In practical geotechnical site characterization, the determination of number of borehole measurements should take consideration of both acceptable level of uncertainty and project budget. For instance, if the percentage change of 1% in the mean of FoS is taken as the termination criterion, 3 boreholes are considered sufficient for slope subsurface stratigraphy and stability evaluation.

6. Effect of MPS training images on slope stability analysis

Training image has significant impact on stochastic simulation results and subsequent slope stability analysis. When all potential stratigraphic relationships of a simulation image are properly reflected by a training image, only relatively limited site-specific measurements (e.g., outcrops or boreholes) are required to properly recover stratigraphic connectivity of the simulation image, and accurate slope stability analysis results can be obtained. Two crucial factors governing training image are thickness of each individual soil layer and curvature of soil layer boundaries. In this section, three additional training images are generated. Training images in Fig.5c and 5d, i.e., TI1 and TI2, are generated from the original training, i.e., TI0, in Fig. 5b by scaling and flipping, respectively, for investigating effects of training image on slope stability analysis. The scaled training image in Fig. 5c approximately reduces thickness of soil2 and soil3 layers by half, and the

flipped training image in Fig. 5d inverts soil layer boundary curvature. Training image in Fig. 5e, i.e., TI3, is generated following Eq. (4) and the slope is relatively gentle when compared with TI0.

Evolution of the most probable interpolation and associated total entropy conditioning on scaled training image T1 and sparse site-specific measurements are shown in Fig. 11. It can be seen in Fig. 11a that when only outcrop is taken as site-specific measurement, the most probable interpolation resembles the scaled training image in Fig. 5c and has an accuracy of 47.3%. With the addition of new borehole measurements, the overall stratigraphy in Fig. 11a, particularly near the borehole(s), becomes increasingly similar to the underlying true test image in Fig. 5a, and the associated accuracy monotonically increases from 63.2% to 79.0%. However, more boreholes are required to reveal spatial distribution of soil3 and soil4. It is worthwhile to mention that the calculation of accuracy is not possible in practical projects as underlying true test image is not available in reality. On the other hand, entropy may be used as an index of accuracy. Fig. 11b shows the corresponding entropy evolution with borehole number. It is revealed that areas of large entropy values mainly cluster around the interpolated soil boundaries. The borehole location during sequential updating process is automatically determined from total entropy curve shown in Fig. 11c. When the first borehole is installed at a horizontal distance of 15m, the peak total entropy value increases significantly from less than 30 to over 60. Similarly, a sum of total entropy, i.e., the area under the total entropy curve in Fig. 11c, exhibits a surge from about 2317 to over 3800. This can be attributed to the low similarity of about 40% between the scaled training image TI1 and the test image. The measurements (i.e., newly added borehole) are from the test image, and they are not compatible with the training mage, leading to a jump in both peak and sum of total entropy. In other words, the peak and sum of total entropy may be used as an indication of the compatibility between the training image and site-specific measurements and an index for

evaluating suitability of the training image. When the training image used is suitable for a specific site (i.e., the training image and site-specific measurements are compatible), adding site-specific measurements (i.e., the first borehole) leads to decrease in peak and sum of total entropy. In contrast, if the training image used is not suitable for a specific slope, an increase occurs in the peak and sum of total entropy when adding the first borehole. For example, the peak and sum of total entropy increase significantly, when the first borehole is added to the analysis with the training image TI1 (see Fig. 11). This suggests that training image TI1 is not suitable for this specific site and shall be abandoned. Note that, in Fig. 11, the training image TI1 is still used for the second and third borehole to enable a consistent comparison with results from other training images. With the sequential addition of new boreholes, both the peak and sum of total entropy gradually reduces as the increasing amount of site-specific measurements gradually dominate the results.

Similar spatial interpolation results and entropy evolution conditioning on the flipped training image TI2 in Fig. 5d are shown in Fig. 12. When only outcrop is taken as site-specific measurement, the most probable interpolation resembles the training image in Fig. 5d and has an accuracy of about 70.4%. When borehole number increases from 1 to 3, the soil stratigraphic boundaries, particularly soil2 layer, become increasingly similar to the test image with overall accuracy increasing to 80.3%. Meanwhile, entropy zones around the added boreholes in Fig. 12b shrink significantly. Similar to Fig. 11, both the peak and sum of total entropy in Fig. 12 show a sudden jump when the first borehole is added. This indicates that the flipped training image TI2 is not suitable for this specific site.

Fig. 13 shows the spatial interpolation results for another training image, i.e., TI3, in Fig. 5e with a gentle slope. As shown in Fig. 13a, the interpolation accuracy monotonically increases from

about 78% to close to 100% when borehole number increases from 0 to 3. The high accuracy can be attributed to the high similarity, i.e., 92.8%, between TI3 and the underlying test image. The associated entropy bands in Fig. 13b cluster around the interpolated soil boundaries. The peak and sum of total entropy shown in Fig. 13c reduce consecutively. This indicates that TI3 is a suitable training image for this specific site.

Fig. 14a shows an evolution of the sum of total entropy when using different number of boreholes and training images. Clearly, when TI0 and TI3 are used as training images, the resulted sum of total entropy exhibits a monotonic reduction as borehole number increases. In comparison, the calculated sum of total entropy increases when the first site-specific borehole is combined with the training image TI1 or TI2, for stochastic simulation. As mentioned above, a qualified training image should lead to a monotonic reduction in the calculated sum of total entropy as borehole number increases. Therefore, TI1 or TI2 should not be used as training image for further stochastic simulation after installing the first borehole since the increase in the sum of total entropy after the first borehole indicates that TI1 or TI2 is not suitable for this specific site (i.e., the training image is not compatible with borehole measurements from the specific site).

The evolution of factor of safety with borehole number using different training images are shown in Fig. 14b. The true FoS of 1.14 from the test image is also superimposed for comparison. It is clear that all the calculated FoS exhibit a reducing trend with increased borehole number. FoS resulting from TI0, TI2 and TI3 converges quickly to the true FoS when the number of boreholes is more than 2. It is worthwhile to mention that although the most probable interpolation conditioning on flipped training image TI2 has a moderate overall accuracy of about 80% as shown in Fig. 12a, the local stratigraphic boundaries around soil2 and soil3 layers greatly improves with sequentially added boreholes. As slope slip surface mainly passes through soil1, soil2 and soil3

layers, the high local interpolation accuracy results in reasonable estimate of FoS from TI2. In comparison, the scaled training image TI1 leads to an initial FoS of as high as 1.5 when only outcrop is taken as site-specific measurement, and more boreholes are required to make the calculated FoS approach the true FoS.

7. Real slope example

In this section, a slope feature in Tsuen Cam, Hong Kong is collected to illustrate the proposed method. Upgrading works are required to strengthen the slope according to routine a slope check conducted by Hong Kong government. The plan layout of the slope is shown in Fig. 15a. Four boreholes, i.e., DH1, DH2, DH3 and DH4, were carried out for this project. The associated borehole logs are shown in Fig. 15b. Three parallel geological cross-sections were interpreted from the 4 boreholes by practicing geologists for this project (GEO 2001). As only limited boreholes are available, the interpreted slope geological profiles contain certain degree of subjective engineering judgement. In this example, sections B-B and C-C are taken as training and test images, respectively. Both 2D cross-sections are typical weathering profiles in Hong Kong and successively consist of colluvium (Col), residual soil (RS), completely decomposed granite (CDG), highly decomposed granite (HDG) and moderately decomposed granite (MDG). B-B section is considered to contain more stratigraphic information than C-C section, because the outcrop of B-B section has four different soil types (Col, RS, CDG and HDG) as compared with three soil types (Col, RS and CDG) from outcrop of C-C section. Therefore, B-B section is taken as the training image. The horizontal separation between the two cross-sections is about 20m and both profiles have been interpreted by experienced geologists based on limited and sparse boreholes (i.e. three

boreholes in total). Although the underlying true geological profile of the slope feature is not completely known, both cross-sections have been interpreted based on the same engineering principle (i.e., linear interpolation between cross boreholes). Both cross-sections are close to each other and have undergone similar geological processes. Therefore, both interpreted slope profiles are considered to share similar stratigraphic information, and they are used as training and test images, respectively, as shown in Fig. 16. More specifically, the training image was interpreted from three boreholes, i.e., DH1, DH2 and DH4, and the test image was interpreted from only one borehole, i.e., DH4.

Both training and test images in Fig. 16 have a horizontal length and vertical height of 60m and 50m, respectively. The horizontal lengths of B-B and C-C sections within the slope boundary (called engineered slope) shown in Fig. 15 are approximately 50m and 35m. Corresponding resolutions are 0.20m and 0.33m, respectively, resulting in a total of 45000 points. Clearly, both images share common features such as similar spatial connectivity between different soil types and comparable stratigraphic dips. The major differences lie in soil boundaries at slope top and slope toe.

Similar to the simulated example in Section 5, at the start of slope stratigraphy, only "outcrops" of the slope in the test image are taken as measurements. MPS stochastic simulation is carried out following procedures described in section 3. In total, 100 simulations are carried out until the percentage change in the most probable interpolation is less than 0.1% for every 10 additional realizations. The most probable interpolation derived from the 100 realizations is shown in Fig.17a. The interpolated slope profile essentially captures stratigraphic connectivity between different soil types with an overall accuracy of 80.3%. The interpolated soil boundaries look linear as soil boundaries in the training image is interpreted using straight lines connecting boundaries

separating different soils, resulting in limited stratigraphic connectivity in training image. It is worthwhile to mention that true test image is not available in practical site investigation and is used here for validation purpose only. The difficulty discussed in the introduction and illustrated in Fig. 1 is effectively tackled using the proposed method. Entropy map calculated from Eq. (2) is shown in Fig. 17b. Similarly, zones with largest entropy values (i.e., large stratigraphic uncertainty) mainly cluster around stratigraphic boundaries separating different soil layers. When the total entropy value along horizontal direction is examined (see Fig. 17c), a monotonic increase in entropy is observed when the horizontal distance increases from 0 to about 20m. A plateau with peak total entropy values around 18 is observed at a horizontal distance between 20m and 30m, after which total entropy progressively decreases to about 7.5. Following the principle of maximum entropy reduction in Eq. (3), the optimal location of the next borehole is at the horizontal distance of 26.2m.

Fig. 18a shows model setup for slope stability analysis using one slope stratigraphy realization conditioning on crops. Table 4 summarizes the soil parameters adopted for different soil types. The maximum plastic strain-rate upon failure is shown in Fig. 18b. The calculated FoS is 1.100 and associated deep slip surface propagates from slope top to slope toe.

Evolution of the most probable interpolation and the associated entropy map with additional boreholes is shown in Fig.19. When the first borehole is added at the horizontal distance of 26.2m, stratigraphic boundaries at horizontal distance between 0 and 26.2m get constrained and becomes more resemble to the true soil boundary in Fig 16b with an overall accuracy of 85.5%. The updated entropy map in Fig. 19b exhibits a dense entropy contour between 30m and 40m in the horizontal direction, which is consistent with the total entropy curve in Fig. 19c. Similar interpolation results are also observed when the number of boreholes increases to two and three. Accuracy of the most

probable interpolations in Figs. 19d and 19g increases to 88.1% and 92.1%, respectively. In addition, zones of large entropy significantly reduce. Total entropy at points around sampled locations diminishes to zero (see Figs. 19f and 19i). A comparison of the interpreted soil strata along DH4 in Fig. 16b with the most probable profiles conditional on different borehole number is shown in Fig. 20. All the three strata can be reasonably delineated even only outcrop is taken as measurement. The thicknesses of the three soil layers, i.e., CDG, HDG and MDG, from the MPS simulation are consistent with those from the actual profile.

Calculated FoS of all realizations conditioning on different numbers of boreholes are shown in Fig.21. It is obvious that FoS values fluctuate between 1.00 and 1.15. The mean values of FoS monotonically reduce from 1.109 to around 1.057 when borehole number increases from 0 to 3. Similar decreasing trend in terms of standard deviation of FoS is also observed. If 1% change in the mean value of FoS is taken as the termination criterion, three boreholes should be carried out to delineate subsurface stratigraphy.

8. Summary and conclusion

Subsurface stratigraphy is one major task for geotechnical site characterization and plays a key role in evaluating stability of multi-layered soil slopes. The determination of subsurface stratigraphic boundaries for slopes are largely dependent on engineer's prior knowledge of local geology, because the site-specific measurements (e.g., boreholes) are often limited. In addition, conventional sampling strategy normally specifies uniformly spaced boreholes in plan without accounting for stratigraphic uncertainty. There lacks an objective and rational tool for integrating the prior knowledge on slope stratigraphy with site-specific sparse measurements (e.g., outcrops

and limited number of boreholes) and for adaptively determining the optimal locations and number of boreholes for slope stability analysis. In this study, a data-driven smart strategy is proposed to adaptively determine the optimal locations and number of boreholes for slope stability evaluation with proper consideration of stratigraphic uncertainty. The proposed method enables an ensemble of all prior knowledge within a single training image. More importantly, the approach can not only produce slope subsurface stratigraphy even when only limited measurements (i.e., only outcrops without borehole) are available, but also objectively quantify interpolation uncertainty with a single entropy value for easy determination of the optimal location and number of boreholes.

The interpolation process of slope stratigraphy is purely data-driven and does not require any pre-determined function forms. Specification of the optimal borehole location is based on the principle of maximum entropy reduction, which can adaptively specify the optimal location of additional borehole. With the addition of new borehole measurements, the most probable interpolation gets constrained, and multiple realizations become more compatible to measurements. The required total number of boreholes for slope stratigraphy is determined based on the evaluation of the effect of stratigraphic uncertainty on slope stability (e.g., FoS). For a termination criterion of less than 1% change in the estimated FoS, three boreholes are considered sufficient for delineating slope subsurface stratigraphy for engineering design.

Acknowledgements

The authors thank the anonymous reviewers for their valuable comments in improving the quality of this paper. The work described in this paper was supported by grants from the Research Grants

Council of Hong Kong Special Administrative Region, China (Project no. CityU 11213119 and T22-603/15N). The financial support is gratefully acknowledged.

References

Batty, M., Morphet, R., Masucci, P., and Stanilov, K. 2014. Entropy, complexity, and spatial information. Journal of Geographical Systems, 16(4): 363-385.

Boisvert, J.B., Pyrcz, M.J. and Deutsch, C.V. 2007. Multiple-point statistics for training image selection. Natural Resources Research, 16(4), pp.313-321.

Bossi, G., Borgatti, L., Gottardi, G., and Marcato, G. 2019. Quantification of the uncertainty in the modelling of unstable slopes displaying marked soil heterogeneity. Landslides, **16**(12): 2409-2420.

Cai, J., Yeh, T.J., Yan, E., Tang, R., Wen, J., and Huang, S. 2018. An adaptive sampling approach to reduce uncertainty in slope stability analysis. Landslides, **15**(6): 1193-1204.

Ching, J., and Hu, Y. G. 2016. Effect of Element Size in Random Finite Element Analysis for Effective Young's Modulus. Mathematical Problems in Engineering, 2016.

Clayton, C., Matthews, M., and Simons, N. 1995. Site investigation, publisher Blackwell Science, 584p.

Elfeki, A., and Dekking, M. 2001. A Markov chain model for subsurface characterization: theory and applications. Mathematical Geology, **33**(5): 569-589.

Elkateb, T., Chalaturnyk, R., and Robertson, P.K. 2003. An overview of soil heterogeneity: quantification and implications on geotechnical field problems. Canadian Geotechnical Journal, **40**(1): 1-15.

Fadlelmula, F.M.M., Killough, J., and Fraim, M. 2016. TiConverter: A training image converting tool for multiple-point geostatistics. Computers & Geosciences, **96**: 47-55.

GEO (Geotechnical Engineering Office) 2017. Geoguide 2: Guide to Site Investigation.

GEO (Geotechnical Engineering Office) 2001. Stage 3 Study Report S3R 83/2001: Feature No. 7NW-C/C7 Tsuen Kam Road (Route Twisk). 2001.

Gong, W., Tang, H., Wang, H., Wang, X., and Juang, C.H. 2019. Probabilistic analysis and design of stabilizing piles in slope considering stratigraphic uncertainty. Engineering Geology, 259: 105162.

Gong, W., Zhao, C., Juang, C.H., Tang, H., Wang, H. and Hu, X. 2020. Stratigraphic uncertainty modelling with random field approach. Computers and Geotechnics, 125, p.103681.

Guardiano, F.B. and Srivastava, R.M. 1993. Multivariate geostatistics: beyond bivariate moments. *In* Geostatistics Troia'92. *Edited by* Anonymous . Springer. pp. 133-144.

Hansen, L., Eilertsen, R., Solberg, I., and Rokoengen, K. 2007. Stratigraphic evaluation of a Holocene clay-slide in Northern Norway. Landslides, **4**(3): 233.

Itasca, F. 2011. FLAC-Fast Lagrangian Analysis of Continua, Version. 7.0.

Itasca, FLAC2D. 2013. "Version 6 users manuals." *Itasca Consulting Group. Minneapolis, NM* (2013).

Itasca, FLAC2D. 2014. "Version 7.0 users manuals." *Itasca Consulting Group. Minneapolis, NM* (2014).

Jaynes, E.T. 2003. Probability theory: The logic of science. Cambridge university press.

Juang, C.H., Zhang, J., Shen, M., and Hu, J. 2019. Probabilistic methods for unified treatment of geotechnical and geological uncertainties in a geotechnical analysis. Engineering Geology, **249**: 148-161.

Kulhawy, F.H., and Mayne, P.W. 1990. Manual on estimating soil properties for foundation design. Electric Power Research Institution, Palo Alto, Calif. Report EL-6800.

L'Heureux, J., Longva, O., Steiner, A., Hansen, L., Vardy, M.E., Vanneste, M., Haflidason, H., Brendryen, J., Kvalstad, T.J. and Forsberg, C.F. 2012. Identification of weak layers and their role for the stability of slopes at Finneidfjord, northern Norway. *In* Submarine mass movements and their consequences. *Edited by* Anonymous . Springer. pp. 321-330.

Li, D., Jiang, S., Cao, Z., Zhou, W., Zhou, C., and Zhang, L. 2015. A multiple response-surface method for slope reliability analysis considering spatial variability of soil properties. Engineering Geology, **187**: 60-72.

Li, D., Qi, X., Cao, Z., Tang, X., Phoon, K., and Zhou, C. 2016. Evaluating slope stability uncertainty using coupled Markov chain. Computers and Geotechnics, **73**: 72-82.

Li, D., Xiao, T., Cao, Z., Zhou, C., and Zhang, L. 2016. Enhancement of random finite element method in reliability analysis and risk assessment of soil slopes using Subset Simulation. Landslides, **13**(2): 293-303.

Li, Z., Wang, X., Wang, H., and Liang, R.Y. 2016. Quantifying stratigraphic uncertainties by stochastic simulation techniques based on Markov random field. Engineering Geology, **201**: 106-122.

Liu, L., Cheng, Y., Wang, X., Zhang, S., and Wu, Z. 2017a. System reliability analysis and risk assessment of a layered slope in spatially variable soils considering stratigraphic boundary uncertainty. Computers and Geotechnics, **89**: 213-225.

Liu, L., Cheng, Y., and Zhang, S. 2017b. Conditional random field reliability analysis of a cohesion-frictional slope. Computers and Geotechnics, **82**: 173-186.

Liu, L., Cheng, Y., Pan, Q., and Dias, D. 2020. Incorporating stratigraphic boundary uncertainty into reliability analysis of slopes in spatially variable soils using one-dimensional conditional Markov chain model. Computers and Geotechnics, **118**: 103321.

Liu, Q., and Deng, P. 2019. A numerical investigation of element size and loading/unloading rate for intact rock in laboratory-scale and field-scale based on the combined finite-discrete element method. Engineering Fracture Mechanics, 211, 442-462.

Mariethoz, G., and Renard, P. 2010. Reconstruction of incomplete data sets or images using direct sampling. Mathematical Geosciences, **42**(3): 245-268.

Mariethoz, G. and Caers, J. 2014. Multiple-point geostatistics: stochastic modeling with training images. John Wiley & Sons.

Mood, A.M. 1940. The distribution theory of runs, The Annals of Mathematical Statistics, **11**(4): 367-392.

Phoon, K. 2017. Role of reliability calculations in geotechnical design. Georisk: Assessment and Management of Risk for Engineered Systems and Geohazards, **11**(1): 4-21.

Qi, X., Li, D., Phoon, K., Cao, Z., and Tang, X. 2016. Simulation of geologic uncertainty using coupled Markov chain. Engineering Geology, **207**: 129-140.

Sazzad, M. M., Rahman, F. I., and Mamun, M. A. A. 2015. Mesh effect on the FEM based stability analysis of slope. In International Conference on Recent Innovation in Civil Engineering for Sustainable Development (IICSD-2015) (pp. 387-391).

Shannon, C.E. 1948. A mathematical theory of communication. Bell System Technical Journal, **27**(3): 379-423.

Shi, C., and Wang, Y. 2020a. Non-parametric machine learning methods for interpolation of spatially varying non-stationary and non-Gaussian geotechnical properties. Geoscience Frontiers, https://doi.org/10.1016/j.gsf.2020.01.011.

Shi, C., and Wang, Y. 2020b. Non-parametric and Data-driven Interpolation of Subsurface Soil Stratigraphy from Limited Data using Multiple Point Statistics. Canadian Geotechnical Journal, https://doi.org/10.1139/cgj-2019-0843.

Strebelle, S., and Remy, N. 2005. Post-processing of multiple-point geostatistical models to improve reproduction of training patterns. *In* Geostatistics Banff 2004. *Edited by* Anonymous . Springer. pp. 979-988.

Tahmasebi, P. 2018. Multiple point statistics: a review. *In* Handbook of Mathematical Geosciences. *Edited by* Anonymous . Springer. pp. 613-643.

Wang, G., Wang, Y., Lu, W., Zhou, W., Chen, M., and Yan, P. 2016. On the determination of the mesh size for numerical simulations of shock wave propagation in near field underwater explosion. Applied Ocean Research, 59, 1-9.

Wang, H. 2020. Finding patterns in subsurface using Bayesian machine learning approach. Underground Space, **5**(1): 84-92.

Wang, W., Ng, C.W., Hong, Y., Hu, Y., and Li, Q. 2019. Forensic study on the collapse of a high-rise building in Shanghai: 3D centrifuge and numerical modelling. Géotechnique,**69**(10): 1-16.

Wang, X., Wang, H., and Liang, R.Y. 2018. A method for slope stability analysis considering subsurface stratigraphic uncertainty. Landslides, **15**(5): 925-936.

Wang, X. 2019. Uncertainty quantification and reduction in the characterization of subsurface stratigraphy using limited geotechnical investigation data. Underground Space, **5**(2): 125-143.

Wang, Y., Huang, K., and Cao, Z. 2013. Probabilistic identification of underground soil stratification using cone penetration tests. Canadian Geotechnical Journal, **50**(7): 766-776.

Wang, Y., Cao, Z., and Li, D. 2016. Bayesian perspective on geotechnical variability and site characterization. Engineering Geology, **203**: 117-125.

Wellmann, F., and Caumon, G. 2018. 3-D Structural geological models: Concepts, methods, and uncertainties. *In* Advances in Geophysics. *Edited by* Anonymous . Elsevier. pp. 1-121.

Wellmann, J. F., and Regenauer-Lieb, K. 2012. Uncertainties have a meaning: Information entropy as a quality measure for 3-D geological models. Tectonophysics, **526**: 207-216.

Wellmann, J. F. 2013. Information theory for correlation analysis and estimation of uncertainty reduction in maps and models. Entropy, **15**(4): 1464-1485.

Zhao, T., and Wang, Y. 2019. Determination of Efficient Sampling Locations in Geotechnical Site Characterization Using Information Entropy and Bayesian Compressive Sampling. Canadian Geotechnical Journal, **56**(11), 1622-1637.

List of caption

Tables

Figures

Fig.12 Interpolation results using flipped training image TI2: (a) Evolution of most probable interpolation with measurements; (b) Evolution of entropy plot with measurements; (c) Evolution of total entropy curve with measurements

Fig.13 Interpolation results using training image of gentle slope TI3: (a) Evolution of most probable interpolation with measurements; (b) Evolution of entropy plot with measurements; (c) Evolution of total entropy curve with measurements

Fig.14 Comparison of simulation results using different training images: (a) Evolution of sum of total entropy with borehole number; (b) Evolution of the calculated factor of safety with borehole number

Fig.15 Plan layout of a slope in Hong Kong and associated borehole logs (after GEO, 2001): (a) Layout plan of slope feature 7NW-C/C7; (b) Borehole logs

Fig.16 Training and test images for a real slope in Hong Kong: (a) Training image (B-B section); (b) Test image (C-C section)

Fig.17 Results from the proposed data-driven stratigraphy method: (a) Most probable interpolation conditioning on outcrops; (b) Entropy map of multiple stochastic realizations; (c) Information entropy along horizontal distance

Fig.18 Stability analysis of one realization conditioning on slope outcrop information only: (a) Model setup; (b) Plot of maximum plastic strain-rate

Fig.19 Evolution of most probable interpolation and information entropy for real slope example: (a) Most probable interpolation (1 borehole); (b) Entropy map (1 borehole); (C) Total entropy curve (1 borehole); (d) Most probable interpolation (2 boreholes); (e) Entropy map (2 boreholes); (f) Total entropy curve (2 boreholes); (g) Most probable interpolation (3 boreholes); (h) Entropy map (3 boreholes); (i) Total entropy curve (3 boreholes)

Fig.20 Comparison of measured and interpolated soil strata along DH4 profile

Fig.21 Evolution of factor of safety with an increasing number of boreholes

Tables

Table 1. Coefficients for the function $d = a \times h^2 + b \times h + c$

Function ID	a		b		c	
	mean	std.	mean	std.	mean	std.
I	0.05	-0.02	0.5	0.5	2	5
II	0.19		-0.2		-1.5	
III	0.03		0.5		5	
IV	-0.12		8		-1.5	
V	0.06		0.5		10	

Note: *Std. denotes standard deviation.

Table 2. Summary of key input parameters for MPS simulation

Input parameter	Value
Maximum number of data event replicates in training image, m	20
Maximum number of conditional points, n	40
Minimum Euclidean distance, t	0
Maximum number of iterations	10000
Maximum search radius	10000
Number of realizations	100*

Note: * The number is determined when the percentage change in the most probable interpolation results is less than 0.10% with additional 10 realizations.

Table 3. Soil design parameters for simulated slope

ID	Density, kN/m^3	Bulk modulus, MPa	Shear modulus, MPa	Cohesion, kPa	Friction angle, °
Soil1	20	30	10	10	33
Soil2	18	30	10	5	33
Soil3	18	120	40	10	36
Soil4	18	300	100	15	40

Table 4. Soil design parameters for real example

ID	Density, kN/m^3	Bulk modulus, MPa	Shear modulus, MPa	Cohesion, kPa*	Friction angle, °
Col	19	30	10	15	36
RS				10	35
CDG				20	36
HDG		300	100	25	38
MDG				20	40

Note: * The large cohesion values are assumed to account for strengthening effects of soil nails.

Figures

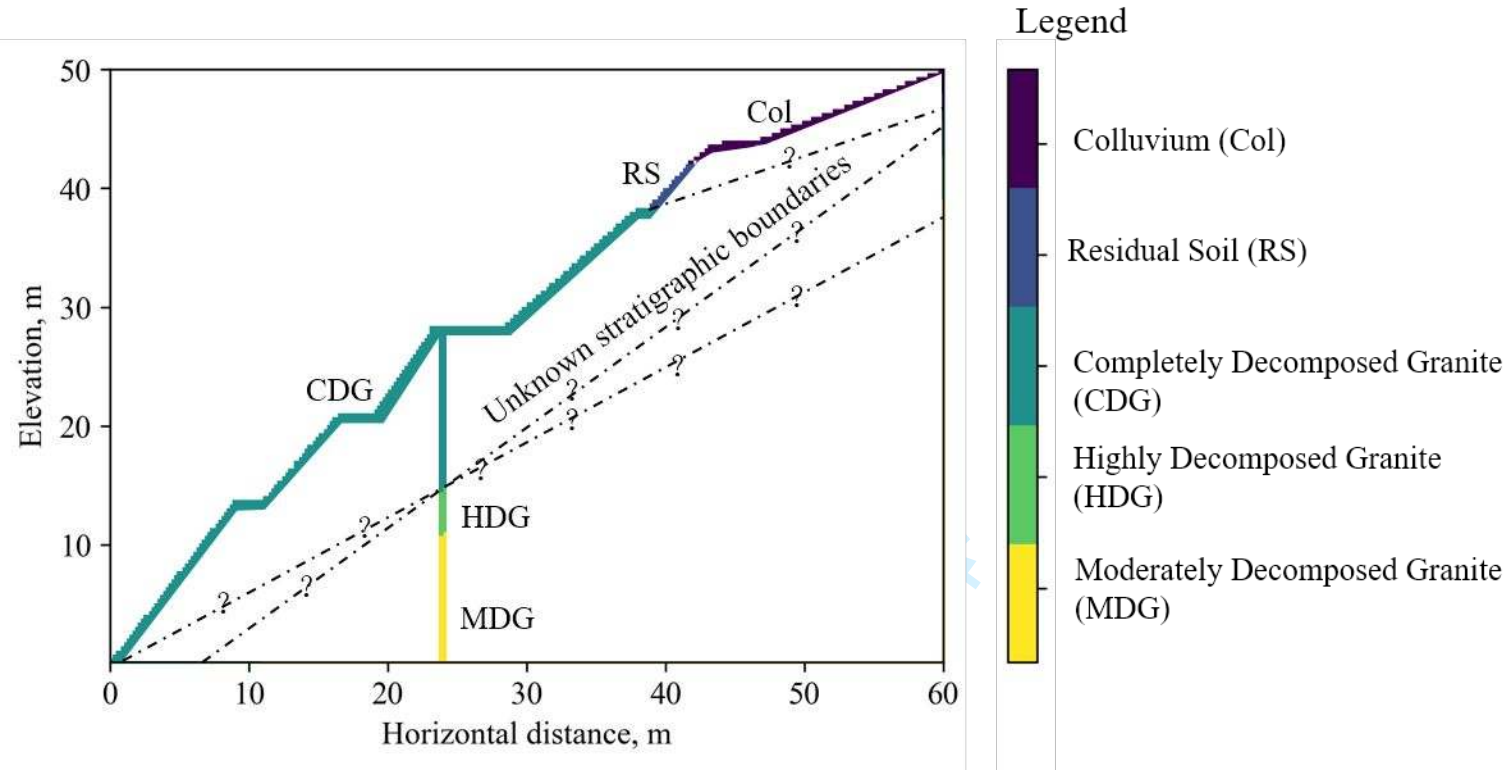

Fig.1. Illustration of a challenge encountered in subsurface stratigraphy from borehole for a real slope in Hong Kong

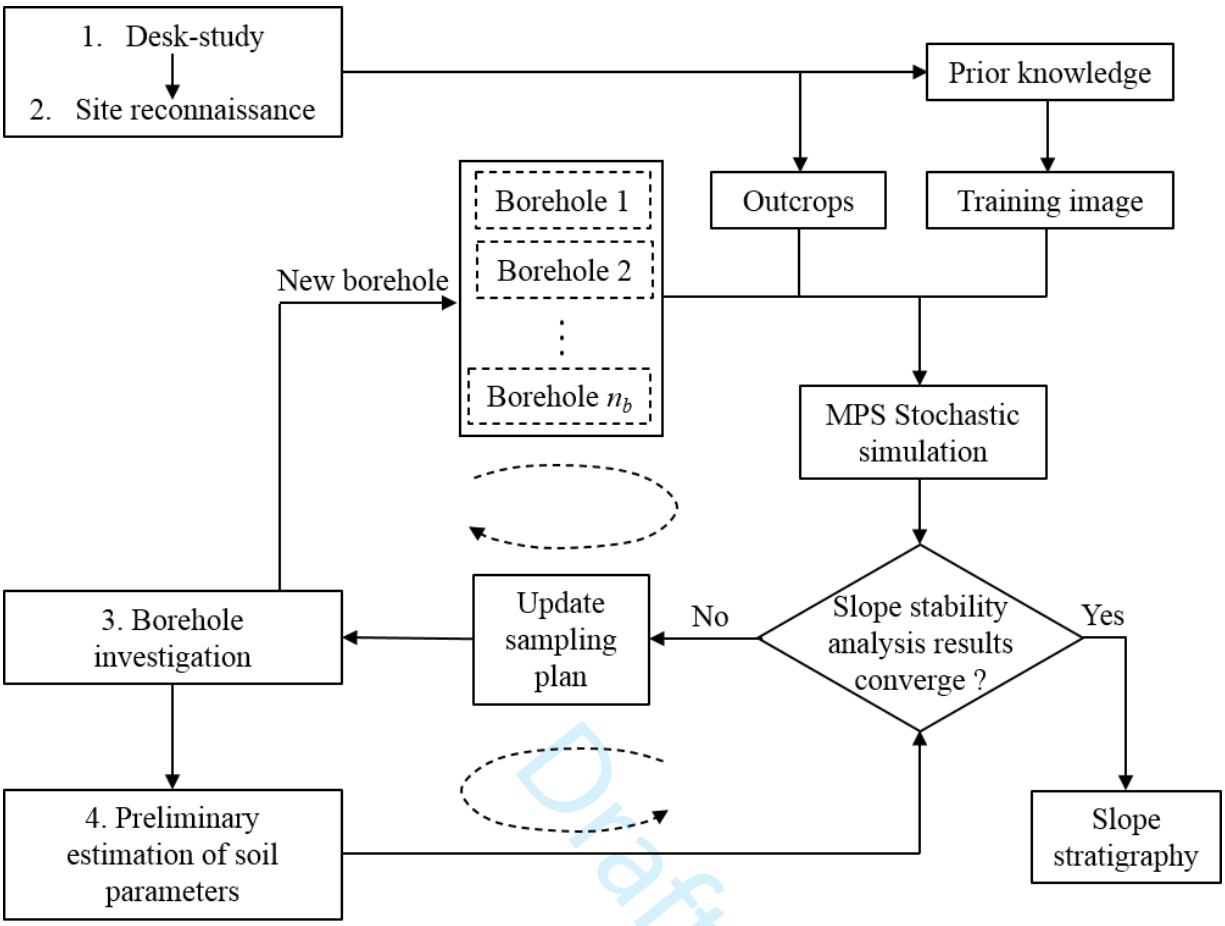

Fig. 2 Proposed data-driven framework for determining optimal locations and number of boreholes for slope stability analysis

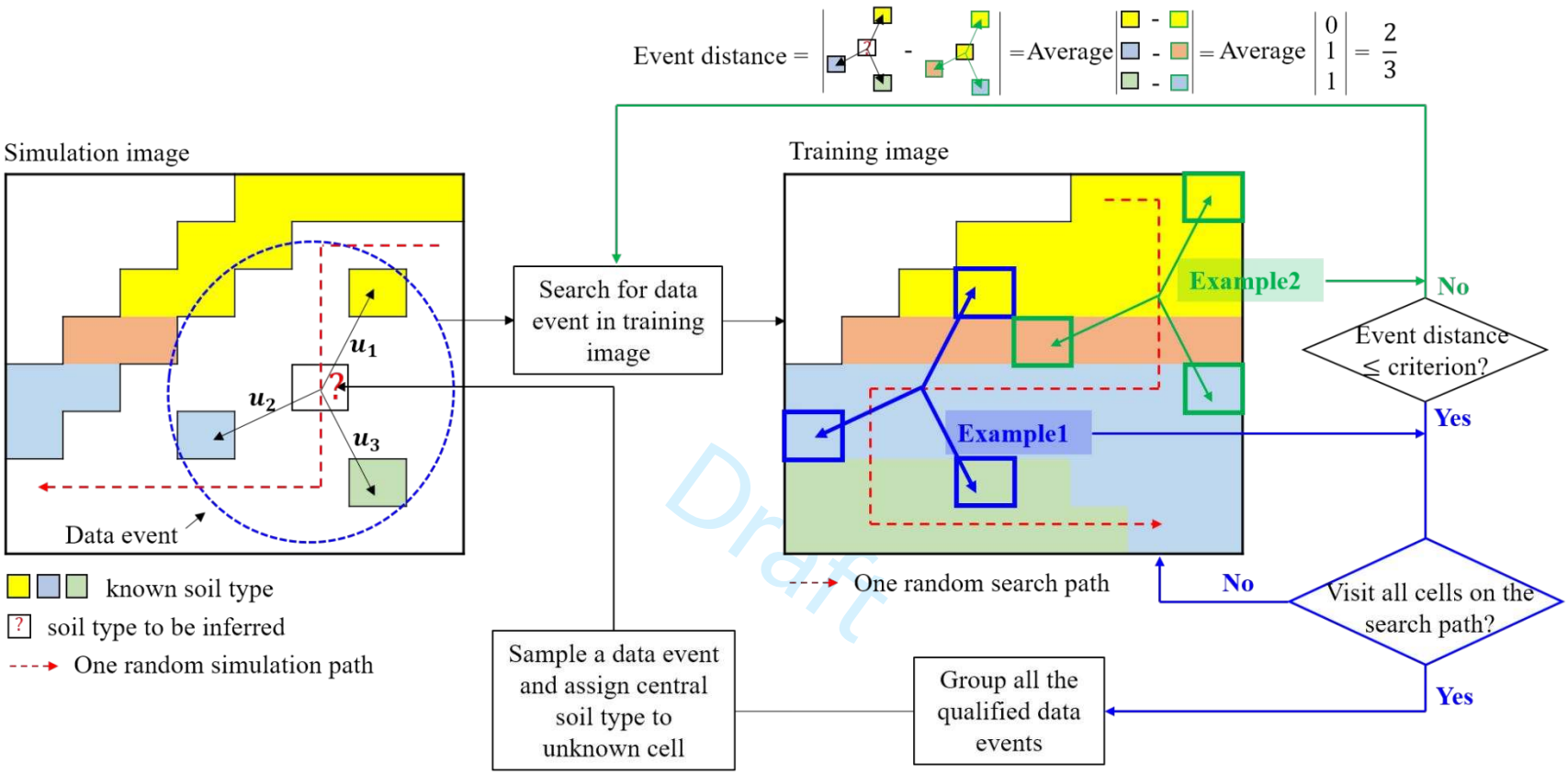

Fig. 3 Illustration of multiple point statistics (after Shi and Wang 2020b)

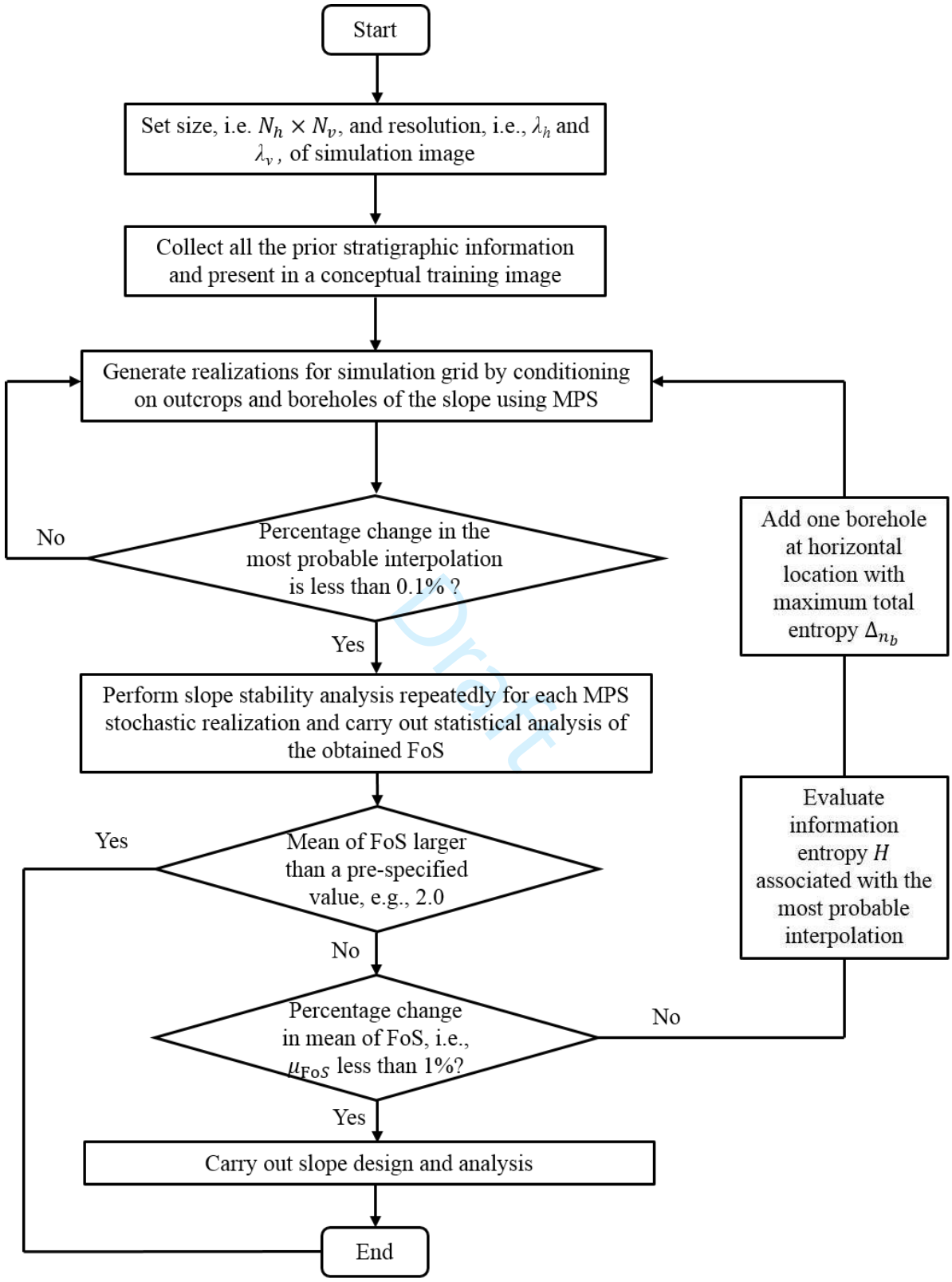

Fig.4 Implementation procedures of the proposed smart sampling strategy

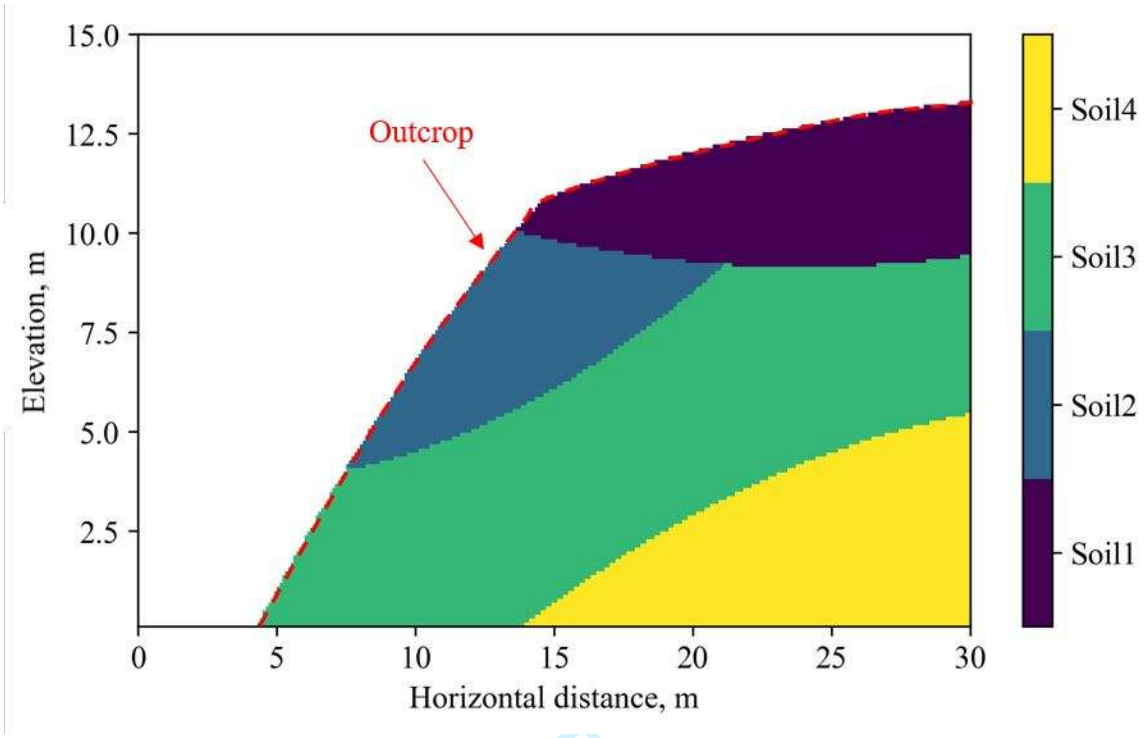

(a) Test image

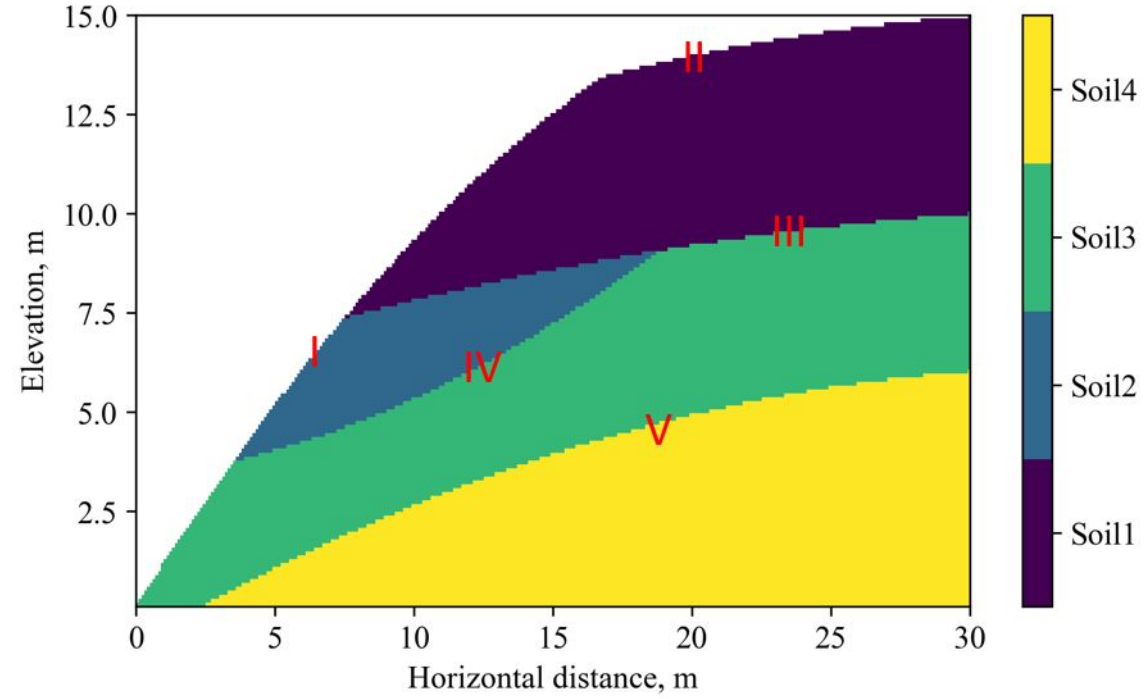

(b) Training image (TI0)

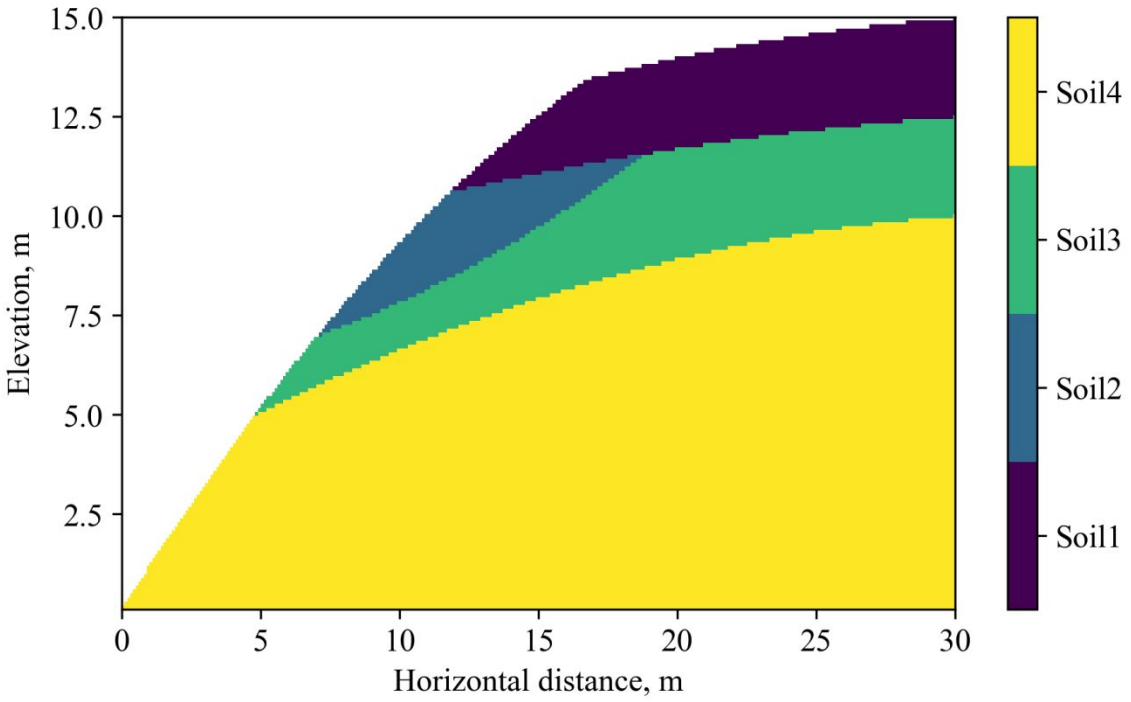

(c) Scaled training image (TI1)

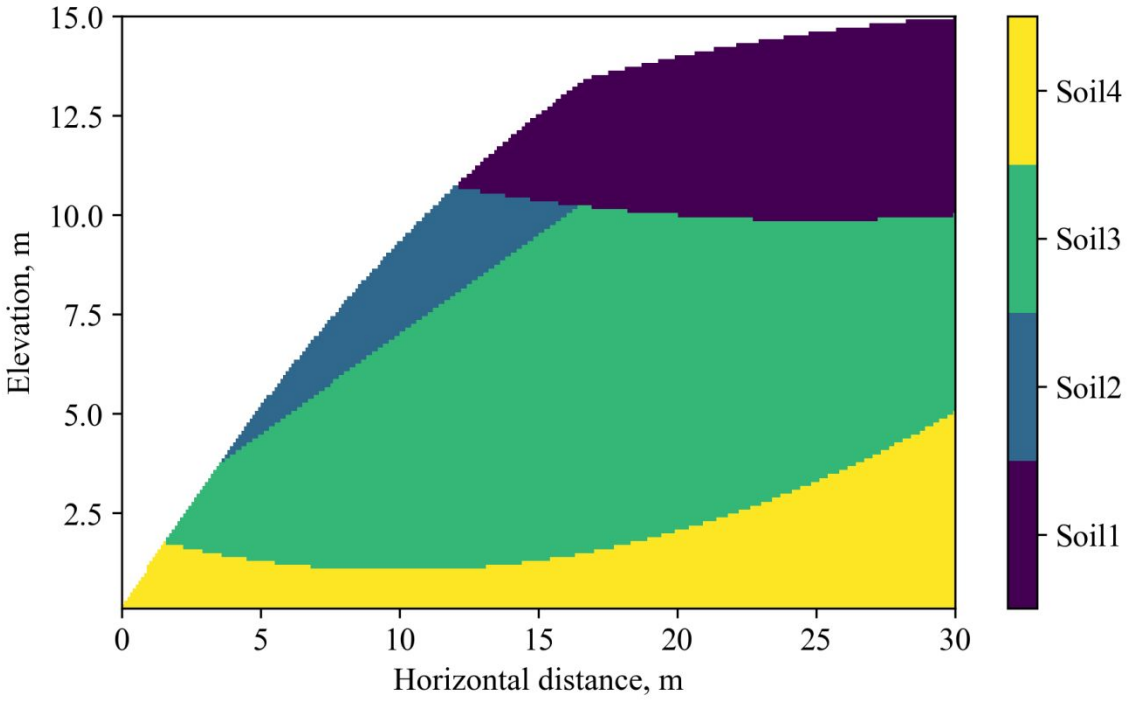

(d) Flipped training image (TI2)

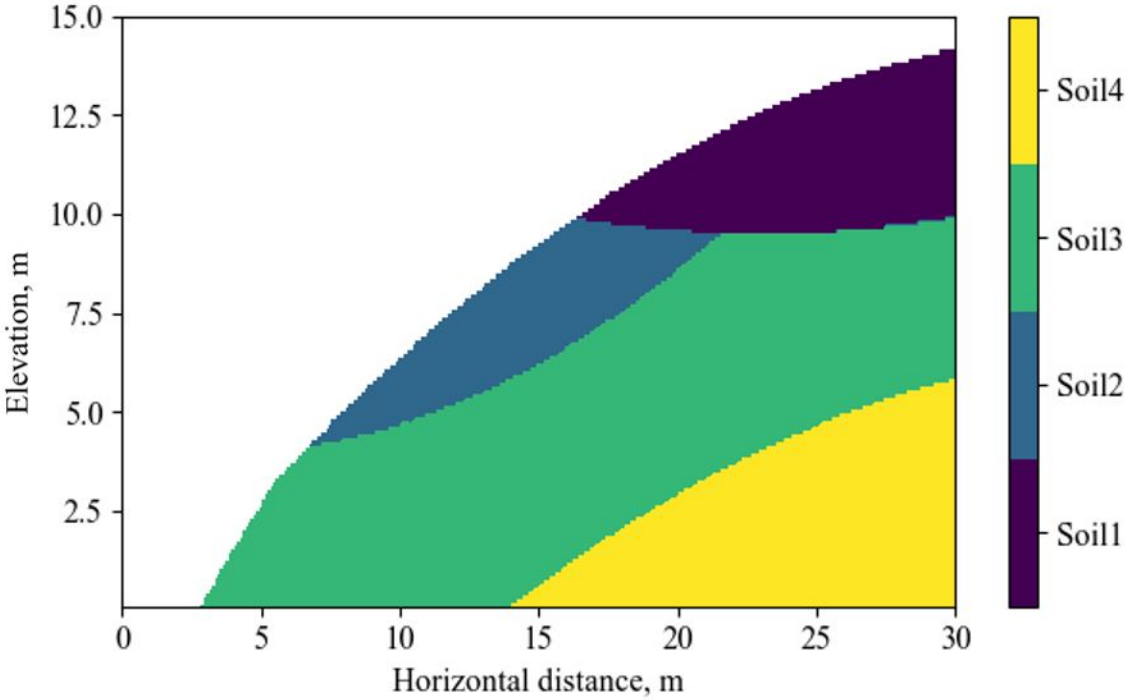

(e) Training image with gentle slope (TI3)

Fig.5 Illustrations of training and test images for the simulated slope example: (a) Test image; (b) Training image (TI0); (c) Scaled training image (TI1); (d) Flipped training image (TI2); (e) Training image with gentle slope (TI3)

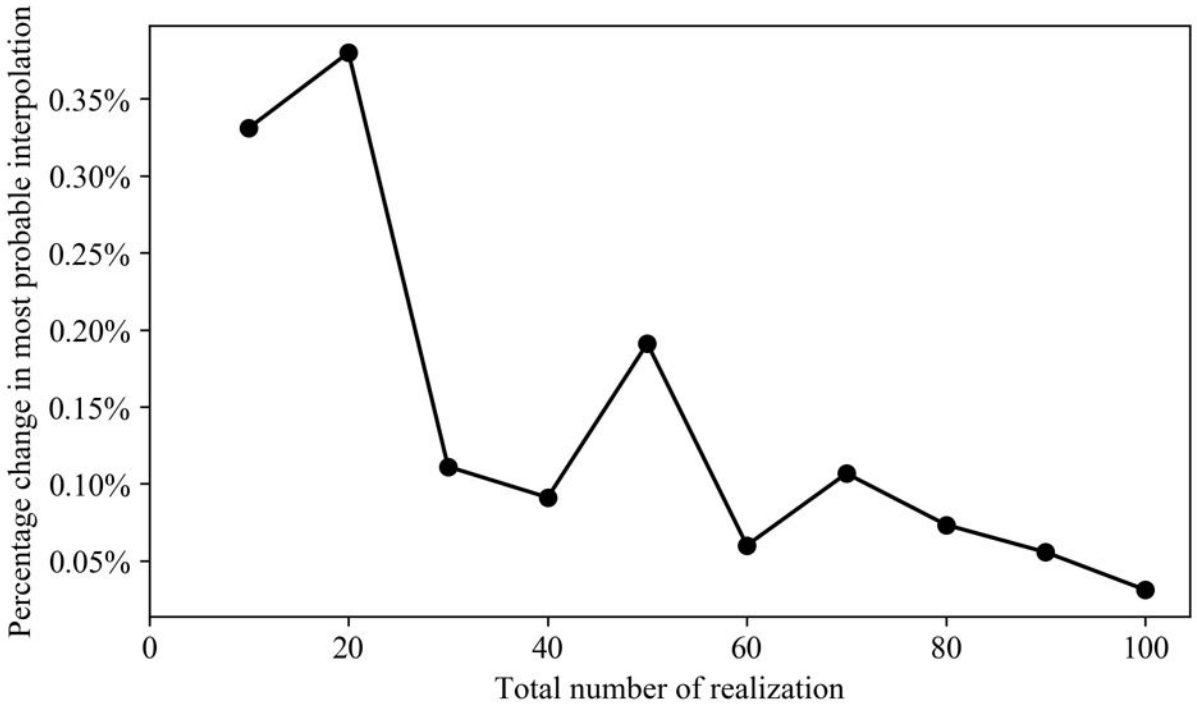

(a) Evolution of percentage change in the most probable interpolation

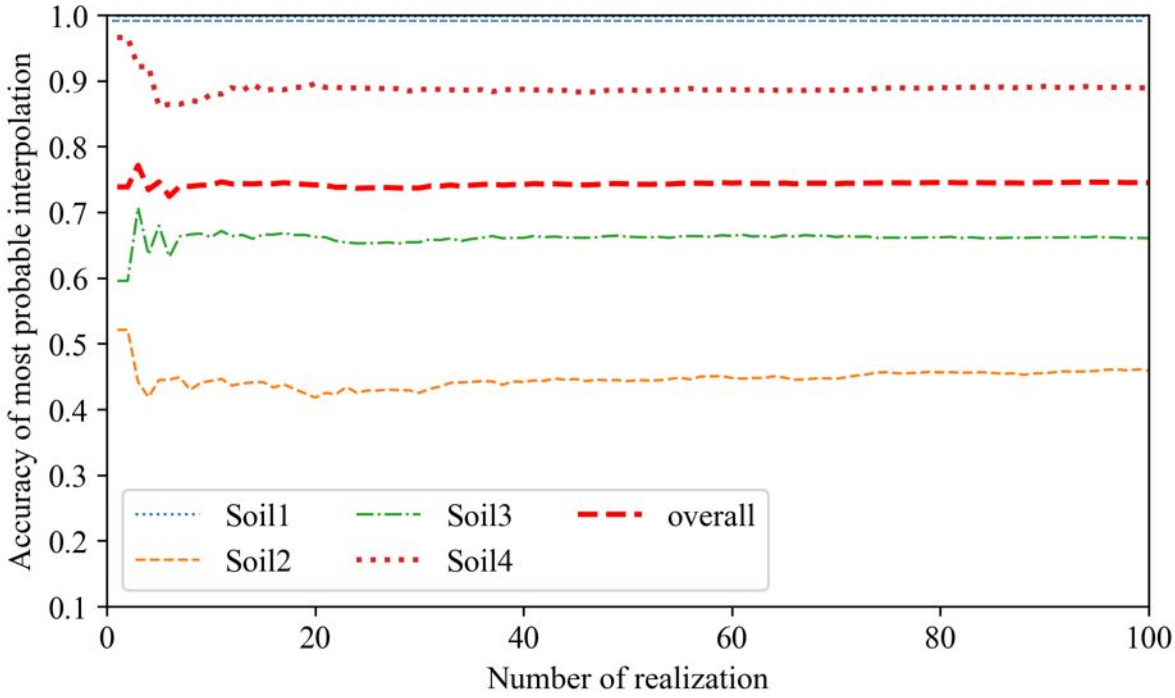

(b) Evolution of accuracy of most probable interpolation with number of realization

Fig. 6 Monitoring of MPS simulation process

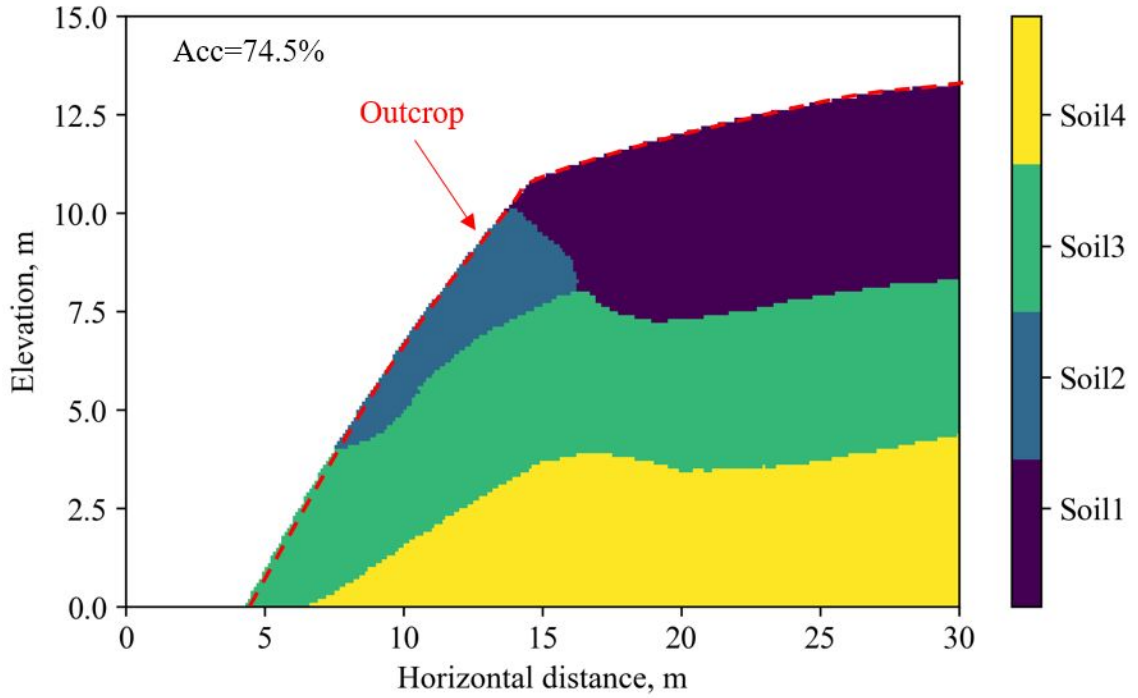

(a) Most probable interpolation conditioning on outcrops only

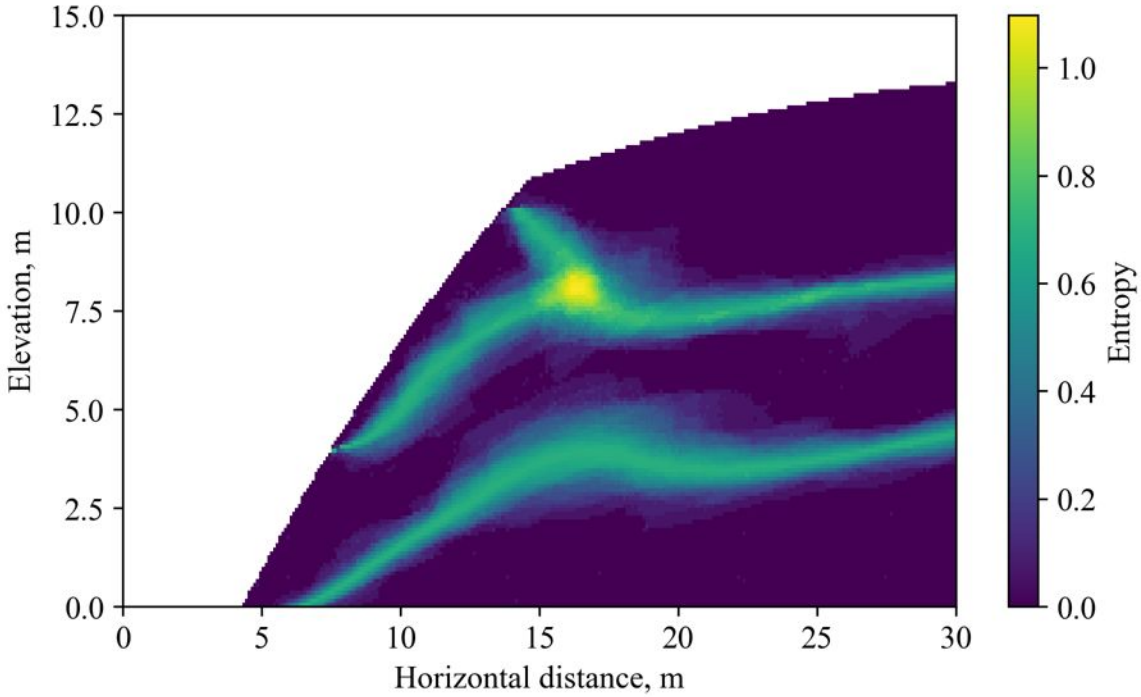

(b) Entropy map from multiple stochastic realizations

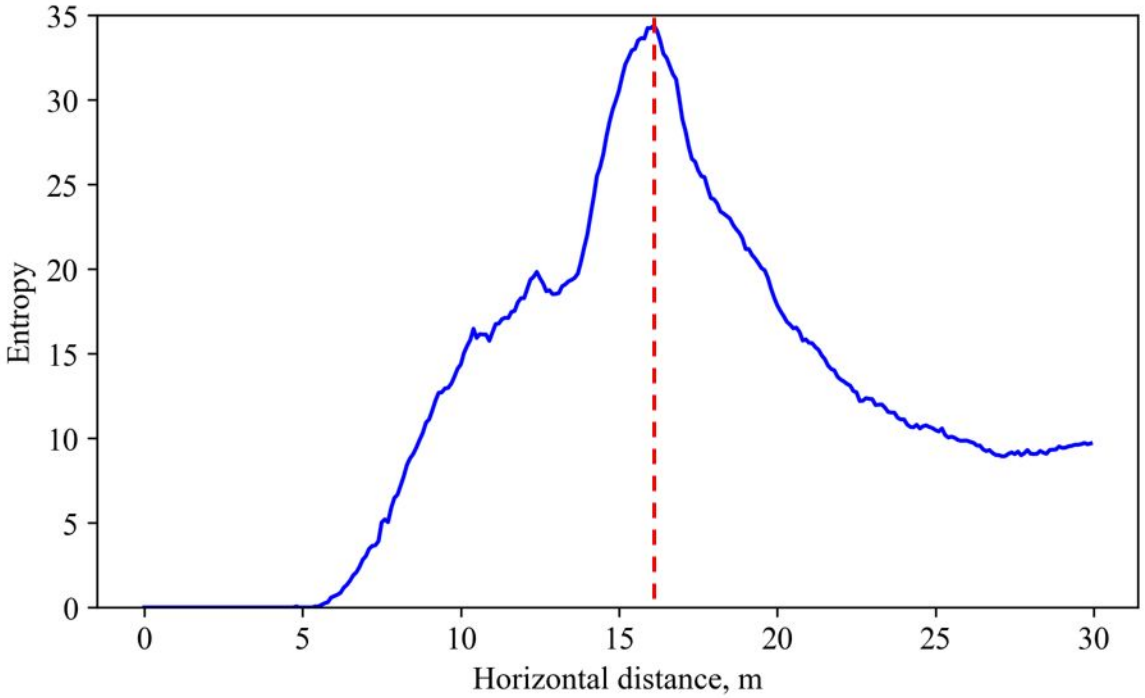

(c) Total entropy along horizontal distance

Fig. 7 Interpolation results from MPS with outcrop information only

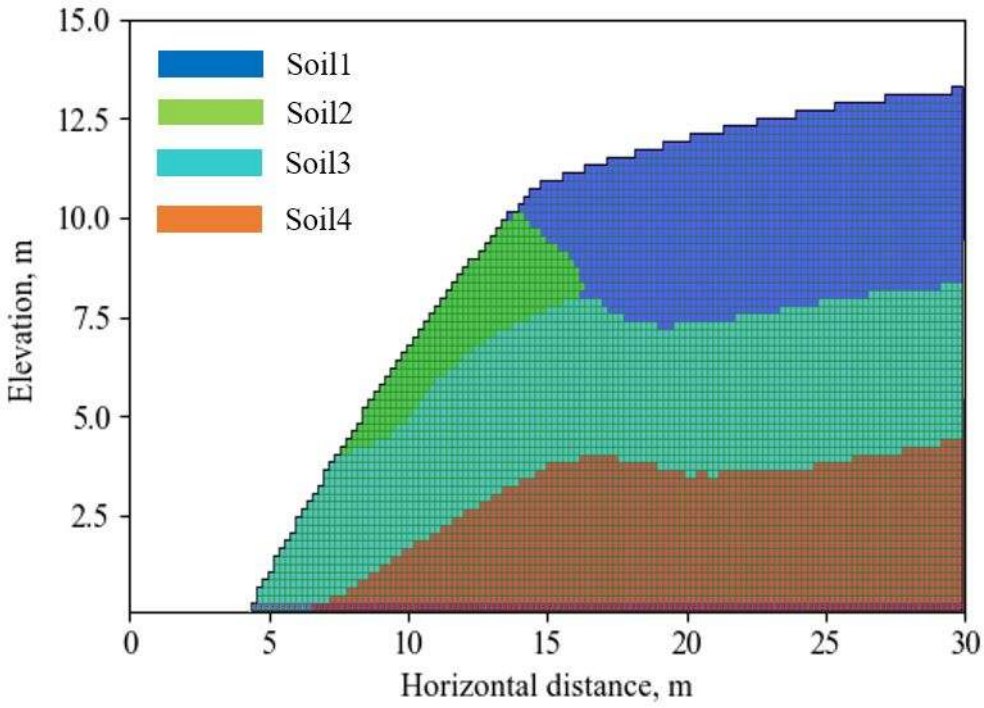

(a) Model setup

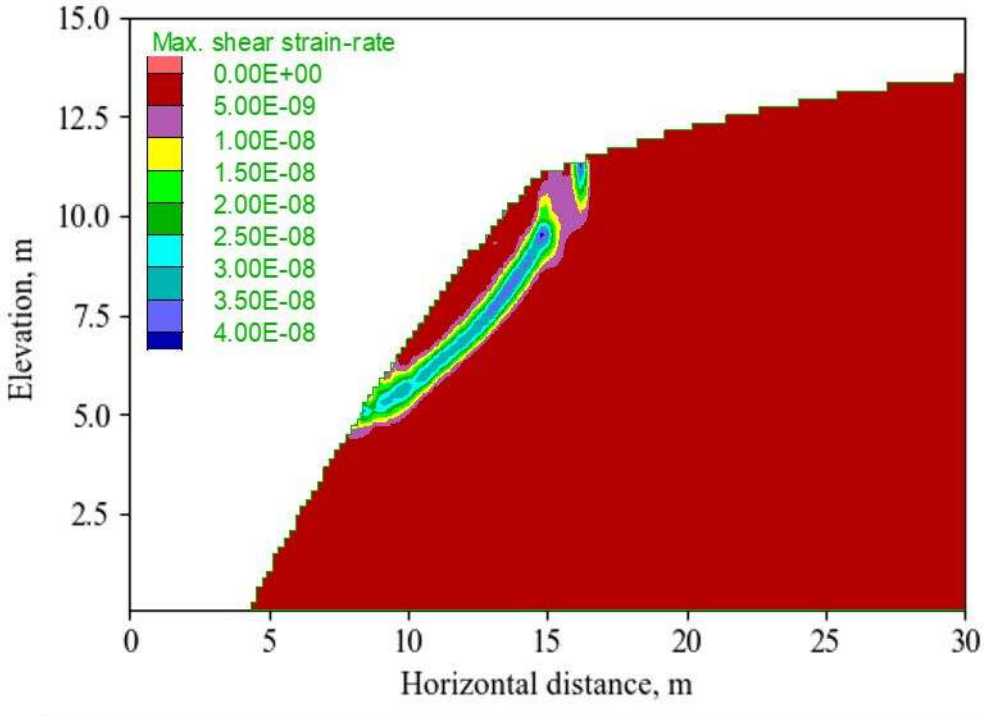

(b) Plot of maximum plastic strain-rate

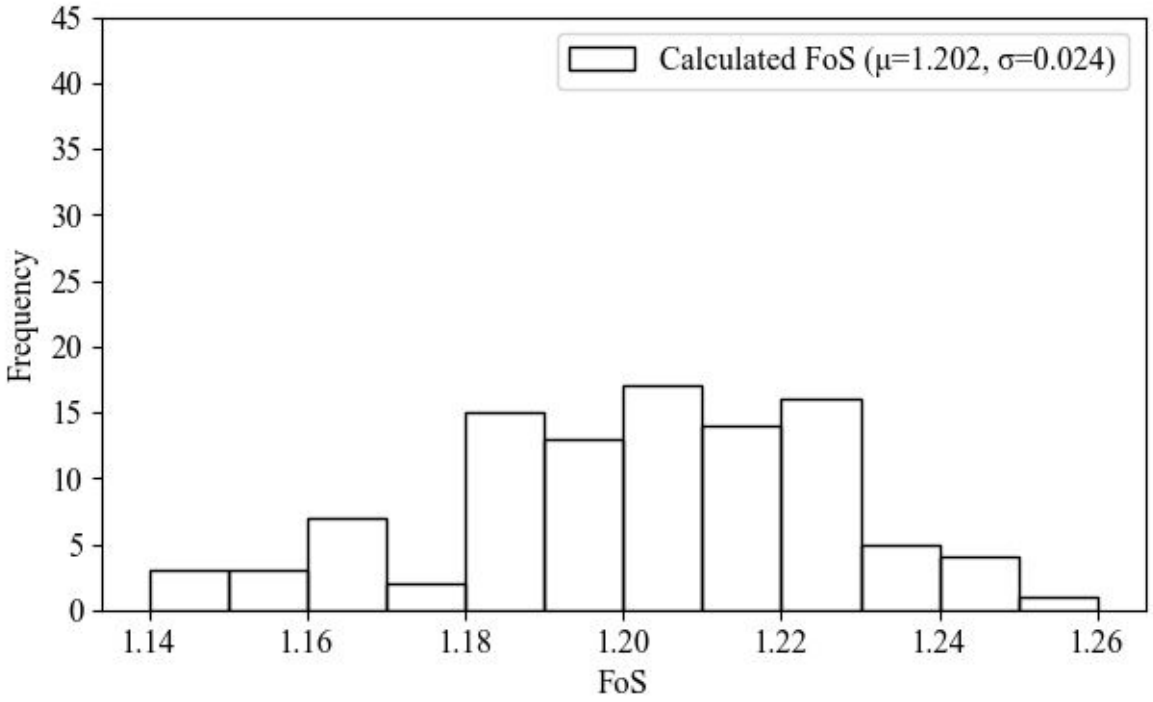

(c) Calculated FoS from 100 realizations

Fig. 8 Slope stability analysis results

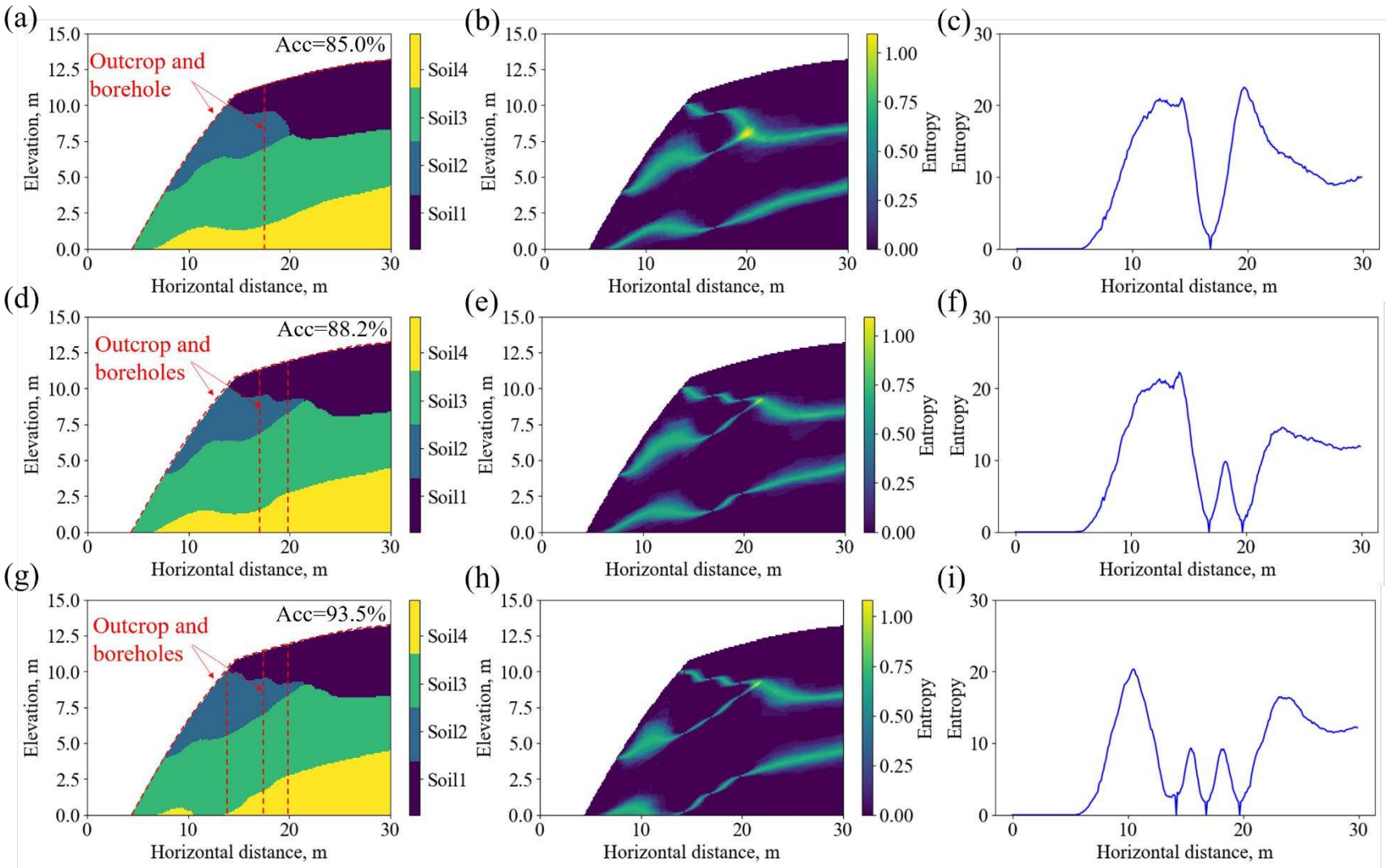

Fig. 9 Evolution of most probable interpolation and total entropy for simulated slope example: (a) Most probable interpolation (1 borehole); (b) Entropy map (1 borehole); (c) Total entropy curve (1 borehole); (d) Most probable interpolation (2 boreholes); (e) Entropy map (2 boreholes); (f) Total entropy curve (2 boreholes); (g) Most probable interpolation (3 boreholes); (h) Entropy map (3 boreholes); (i) Total entropy curve (3 boreholes)

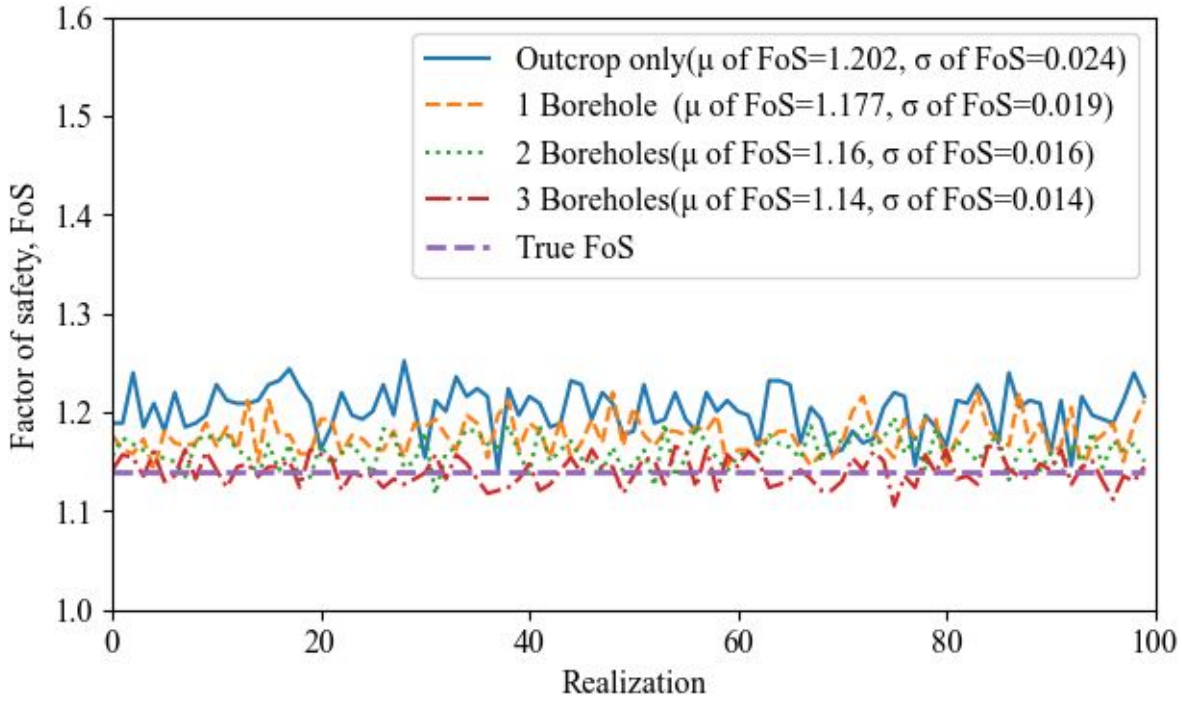

(a) Variation of FoS with realization number

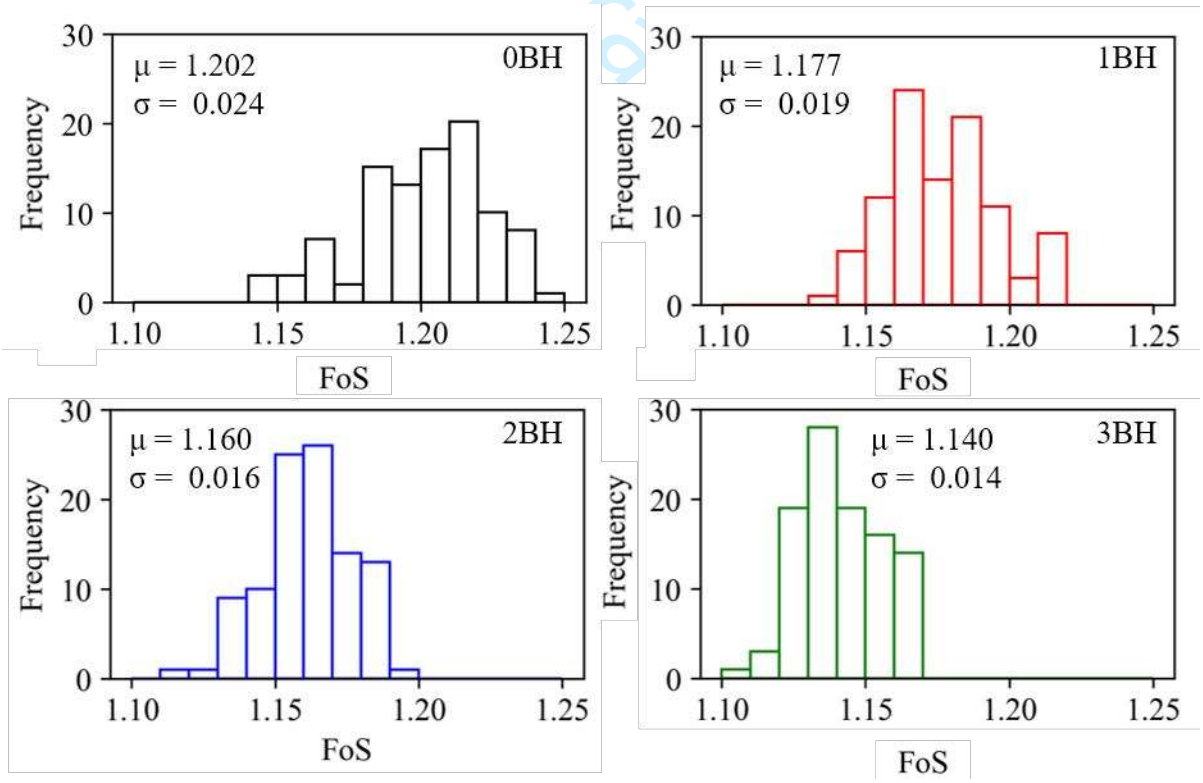

(b) Histogram of FoS for different borehole numbers

Fig. 10 Evolution of factor of safety with an increasing number of boreholes

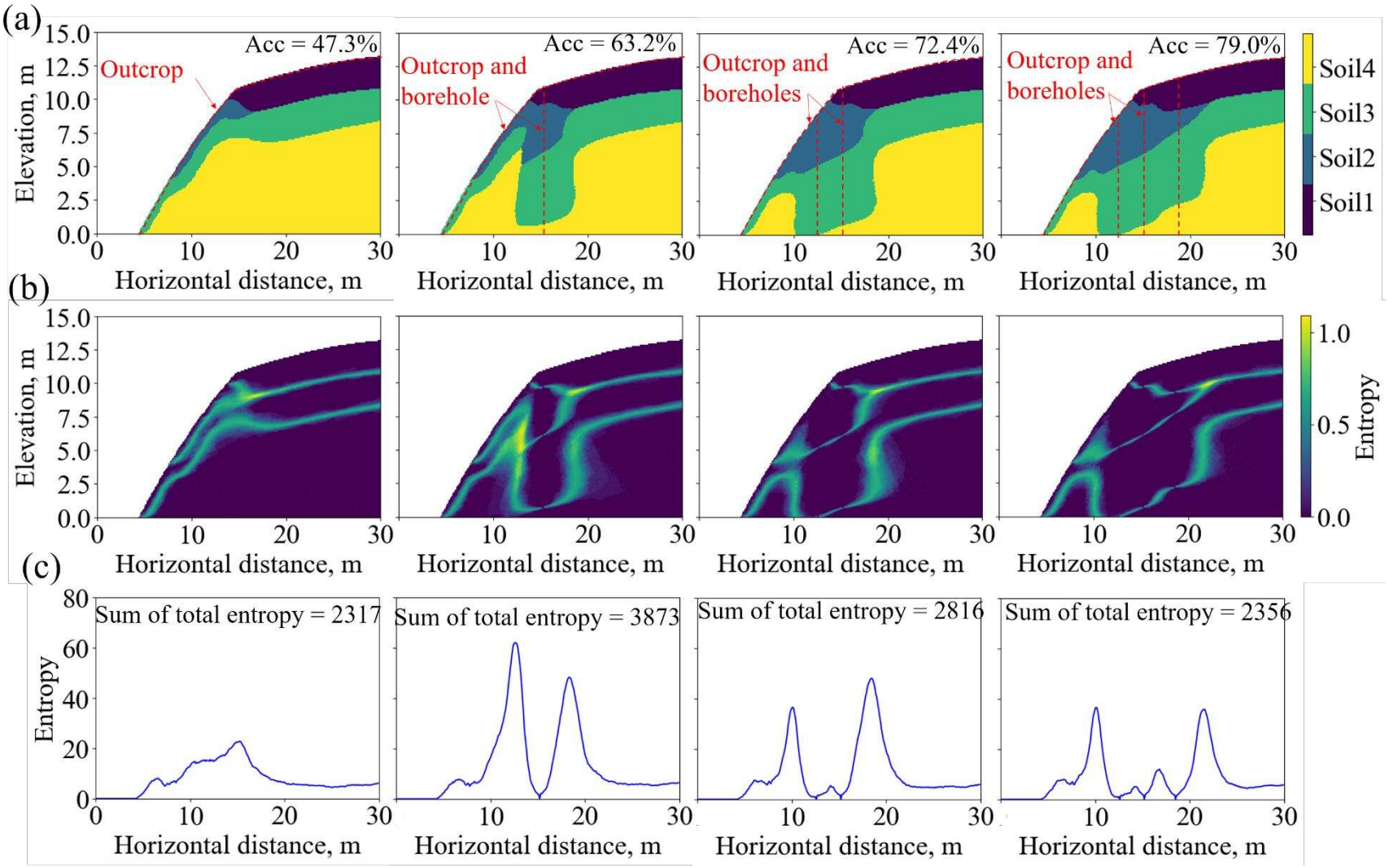

Fig. 11. Interpolation results using scaled training image TI1: a) Evolution of most probable interpolation with measurements; b) Evolution of entropy plot with measurements; c) Evolution of total entropy curve with measurements

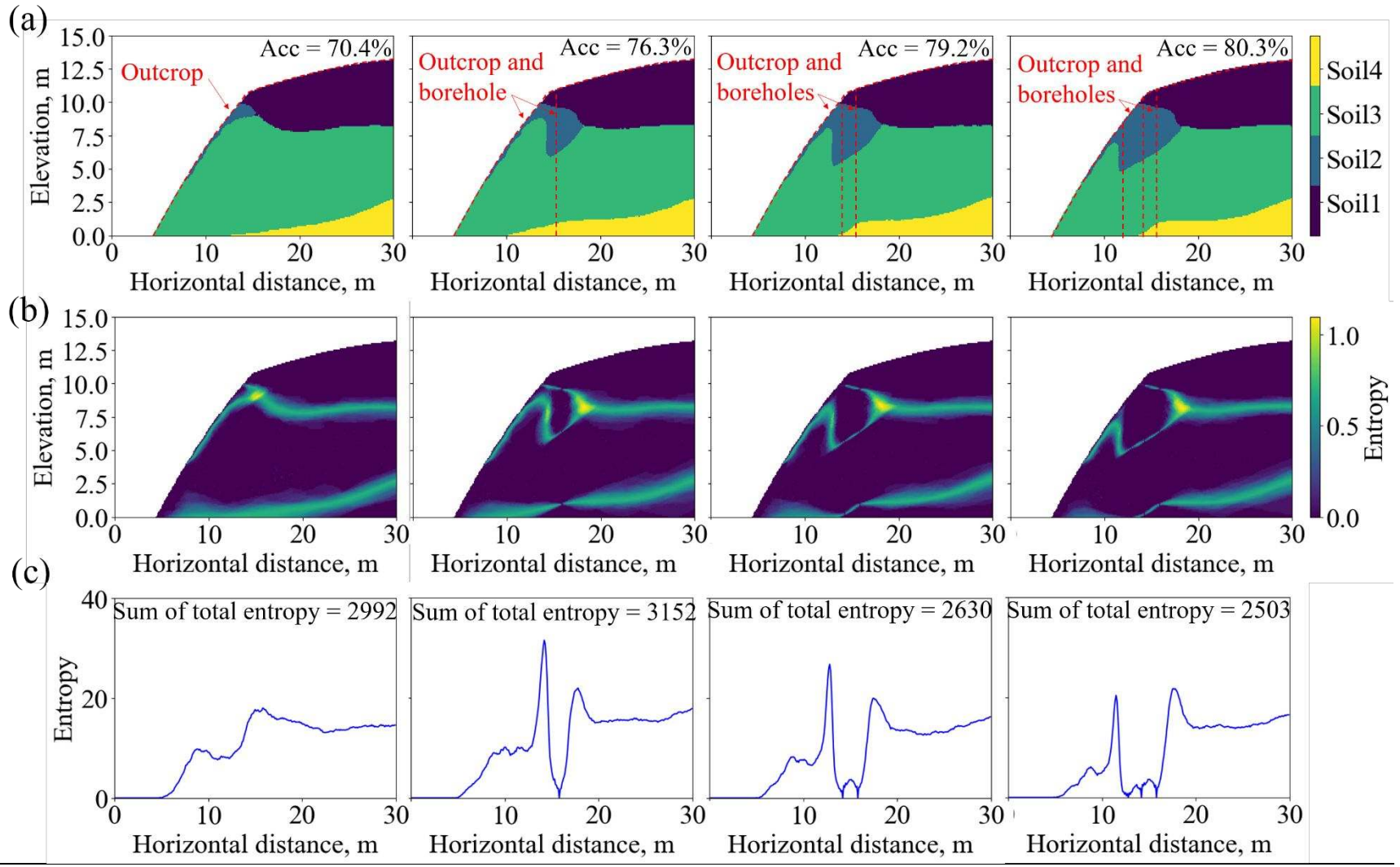

Fig. 12. Interpolation results using flipped training image TI2: a) Evolution of most probable interpolation with measurements; b) Evolution of entropy plot with measurements; c) Evolution of total entropy curve with measurements

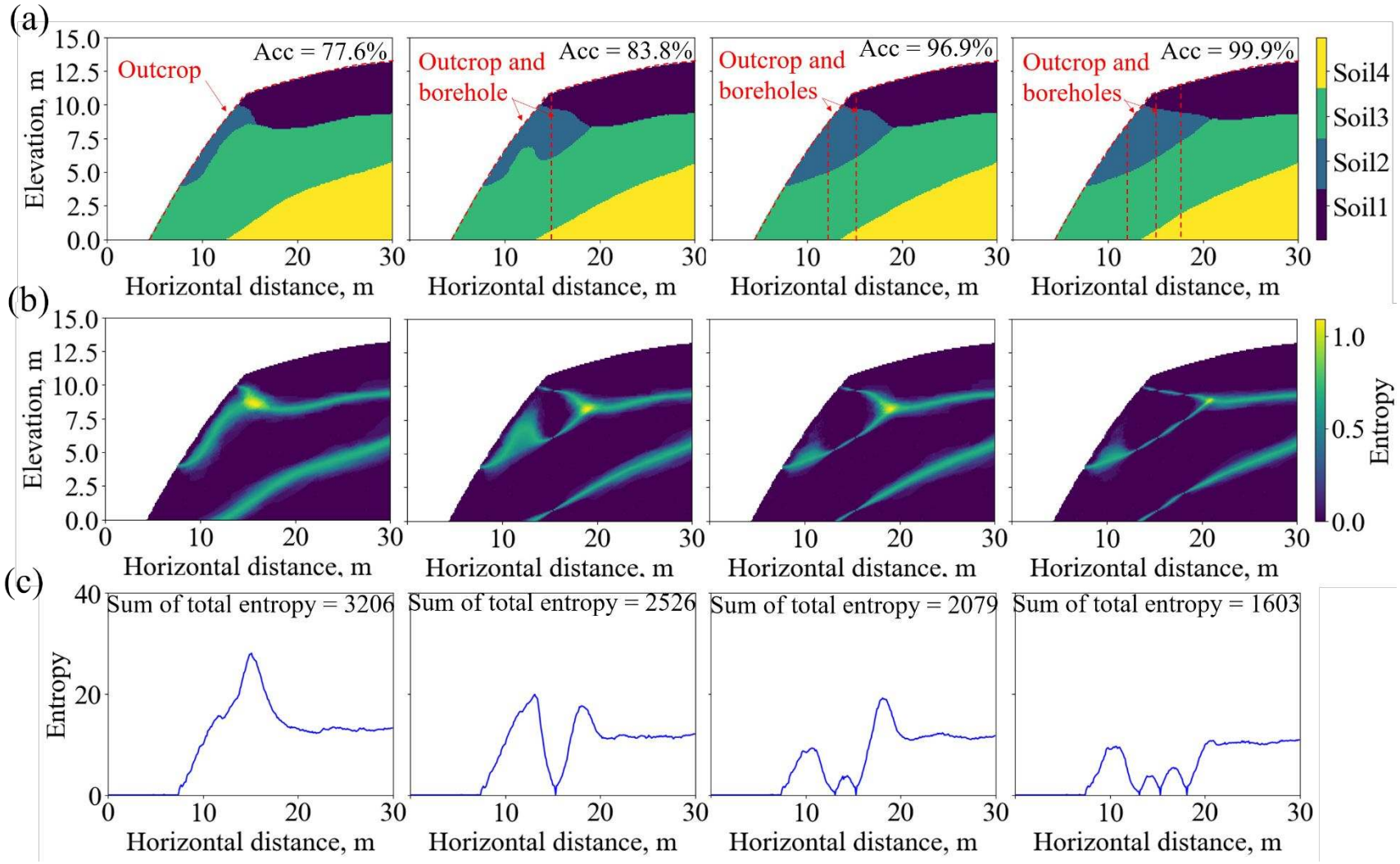

Fig. 13. Interpolation results using training image of gentle slope TI3: a) Evolution of most probable interpolation with measurements; b) Evolution of entropy plot with measurements; c) Evolution of total entropy curve with measurements

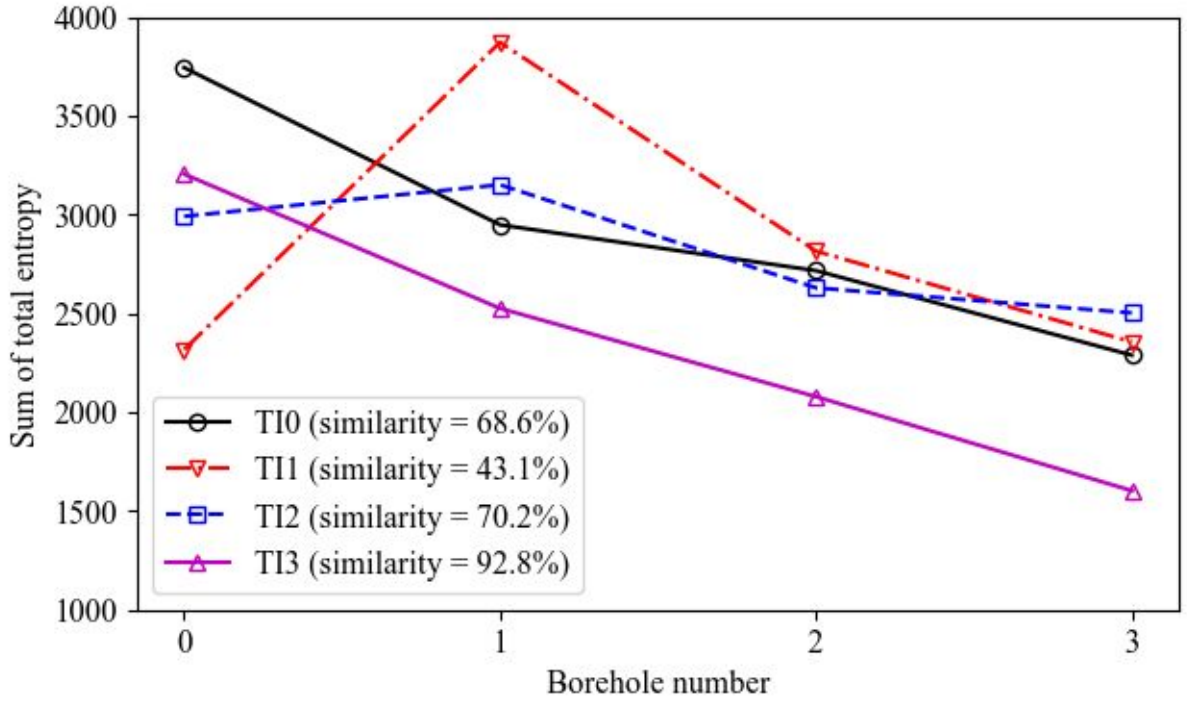

(a) Evolution of sum of total entropy with borehole number

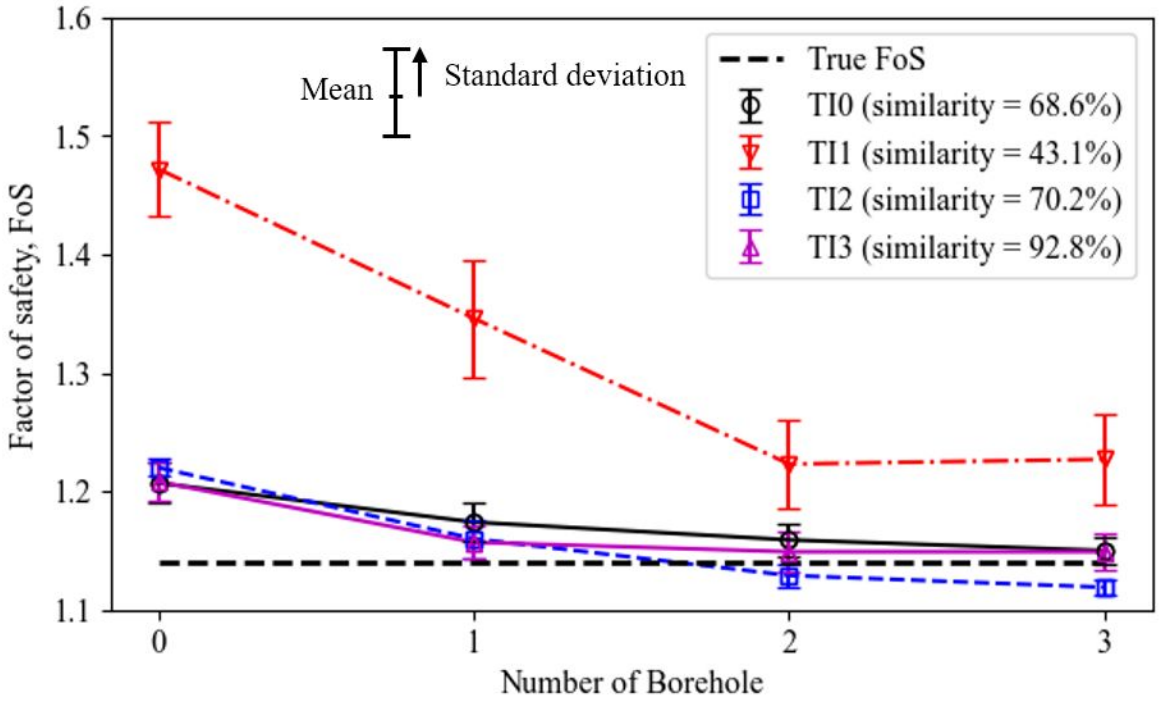

(b) Evolution of the calculated factor of safety with borehole number

Fig. 14. Comparison of simulation results using different training images

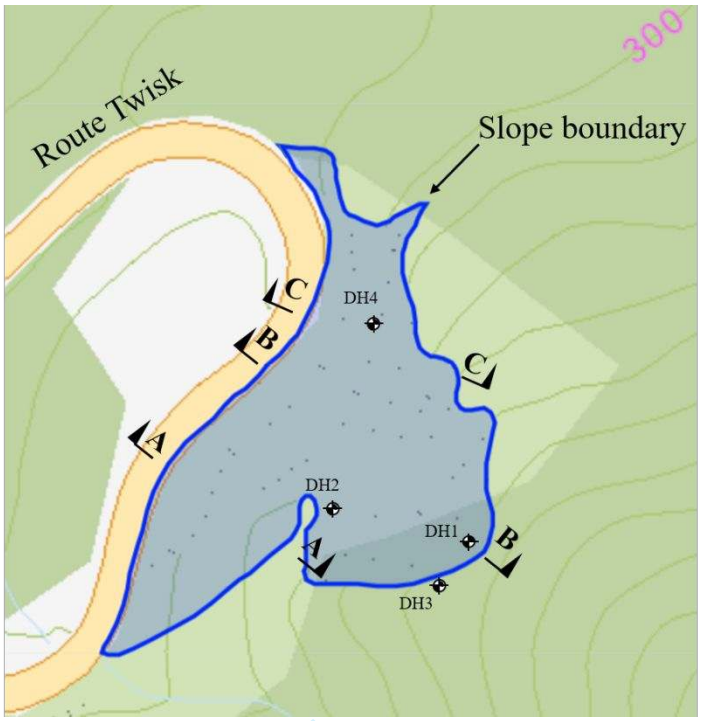

(a) Layout plan of slope feature 7NW-C/C7

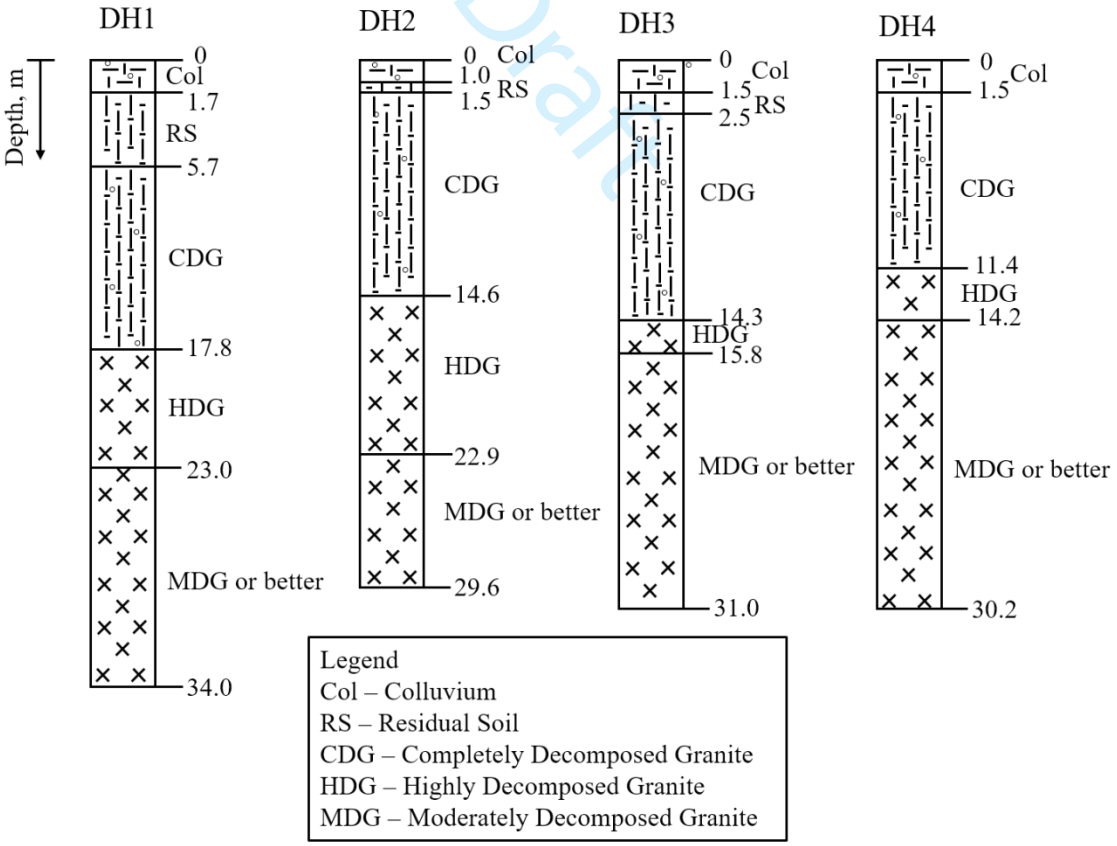

(b) Borehole logs

Fig. 15. Plan layout of a slope in Hong Kong and associated borehole logs (after GEO, 2001)

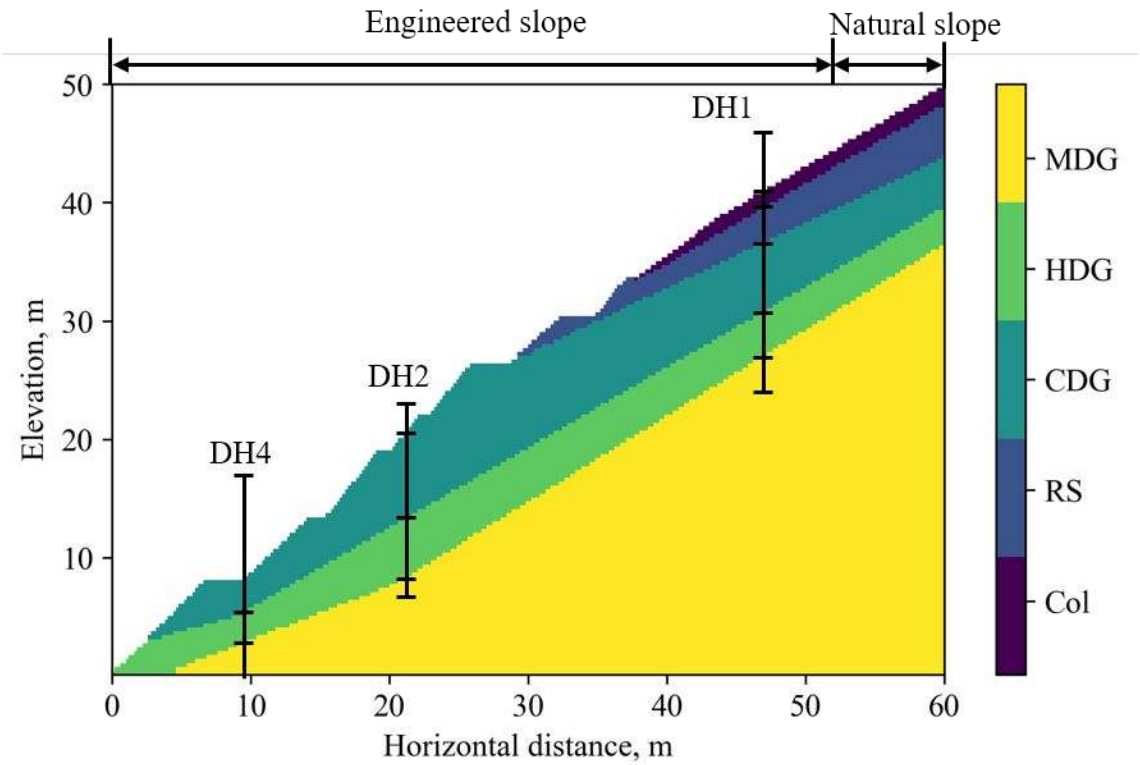

(a) Training image (B-B section)

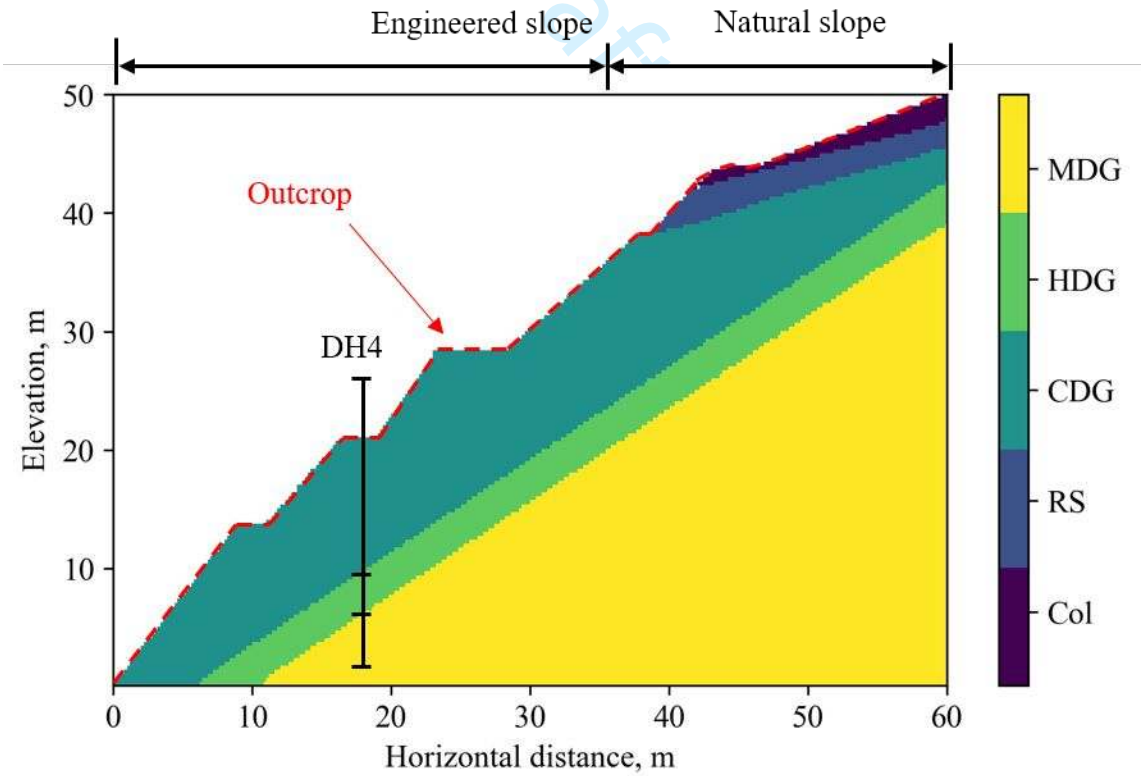

(b) Test image (C-C section)

Fig.16 Training and test images for a real slope in Hong Kong

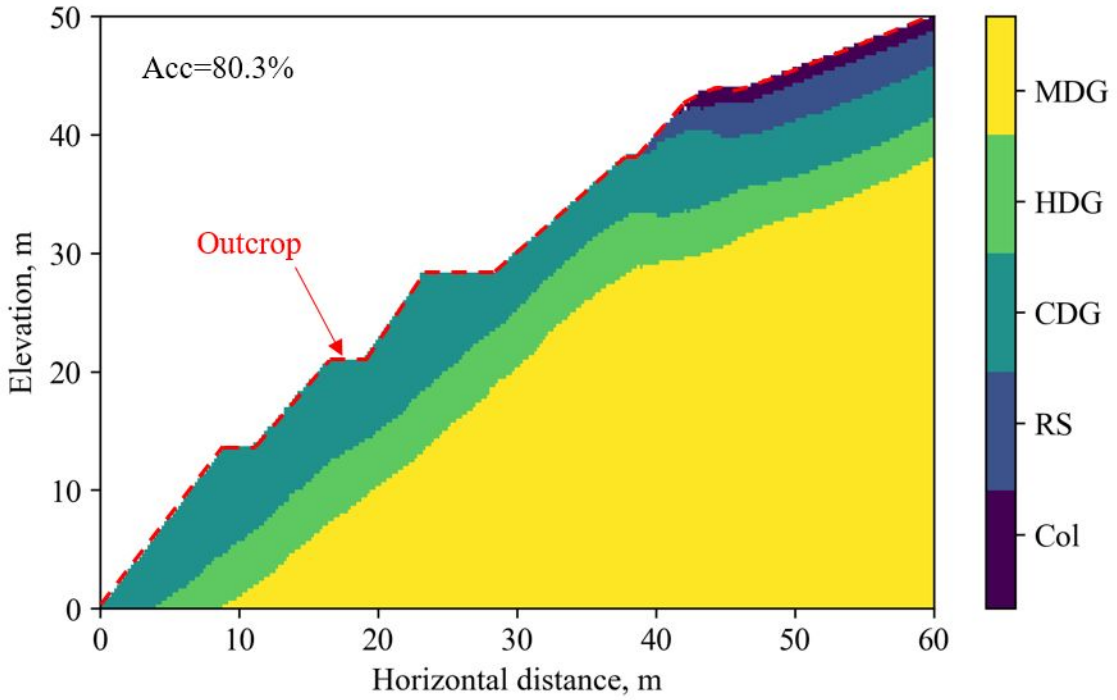

(a) Most probable interpolation conditioning on outcrops

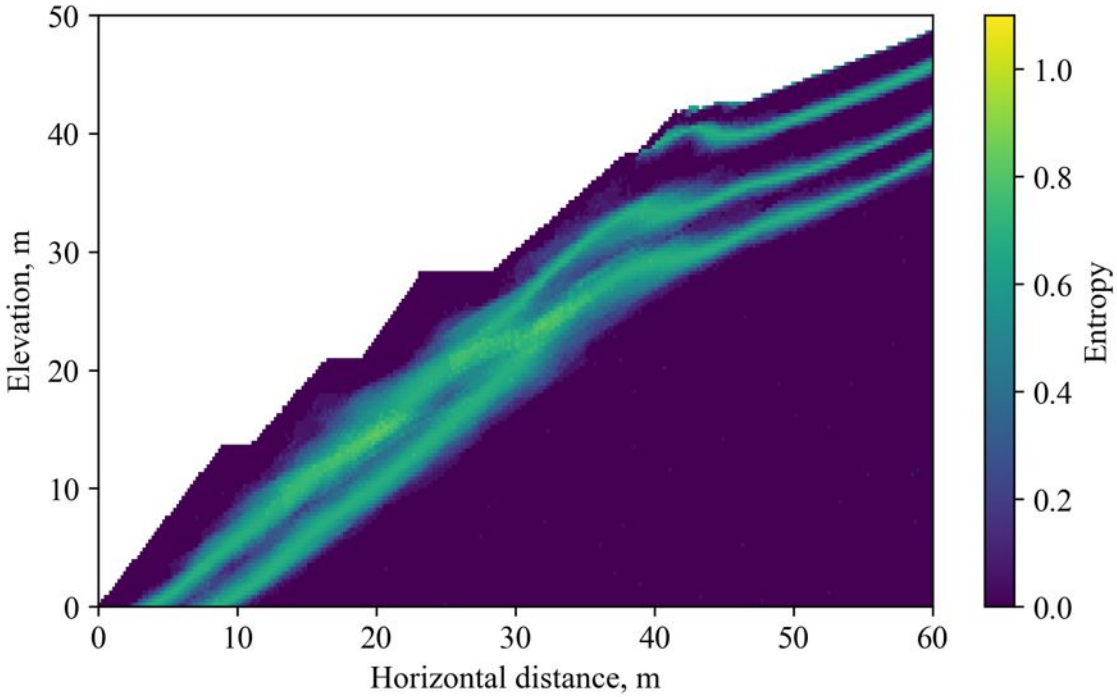

(b) Entropy map of multiple stochastic realizations

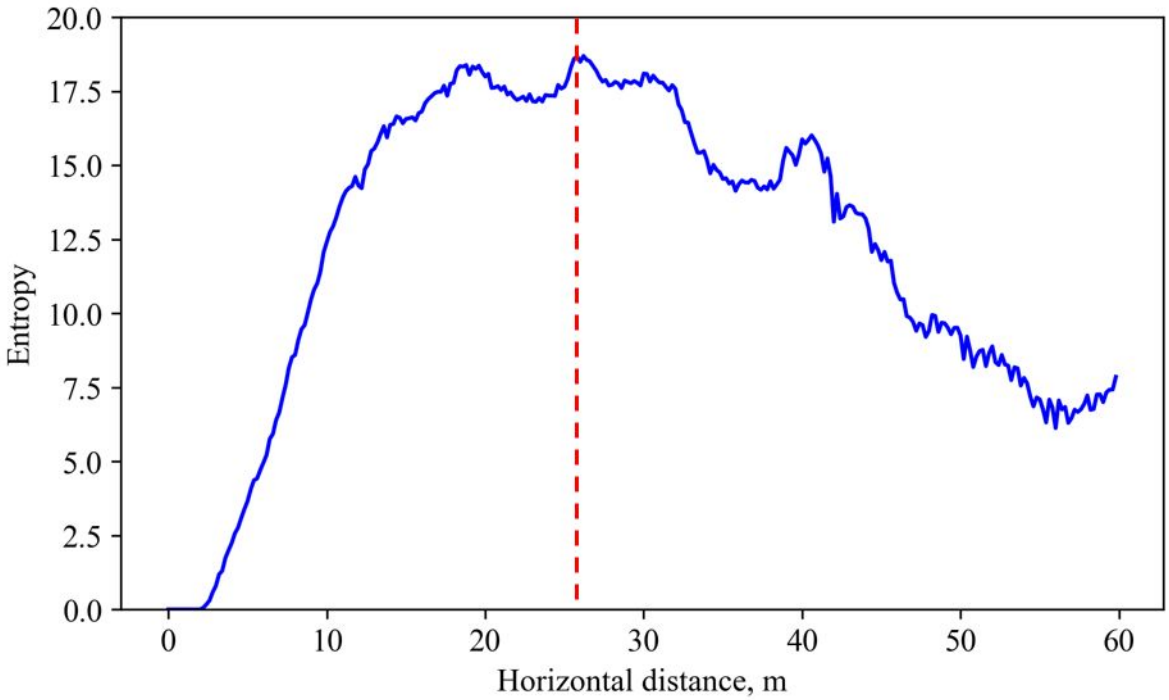

(c) Information entropy along horizontal distance

Fig. 17 Results from the proposed data-driven stratigraphy method

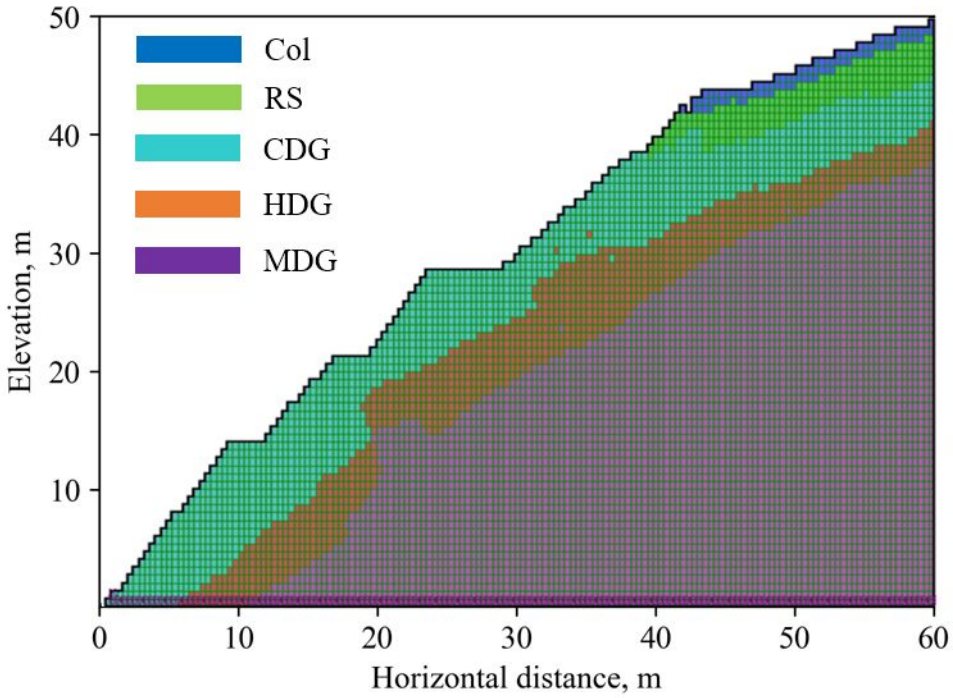

(a) Model setup

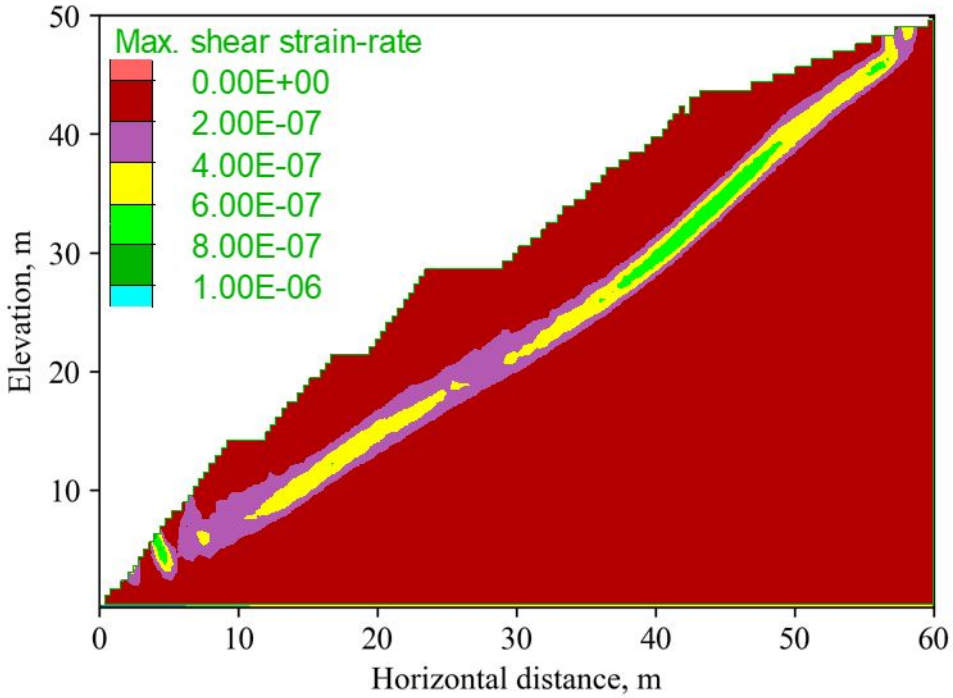

(b) Plot of maximum plastic strain-rate

Fig. 18 Stability analysis of one realization conditioning on slope outcrop information only

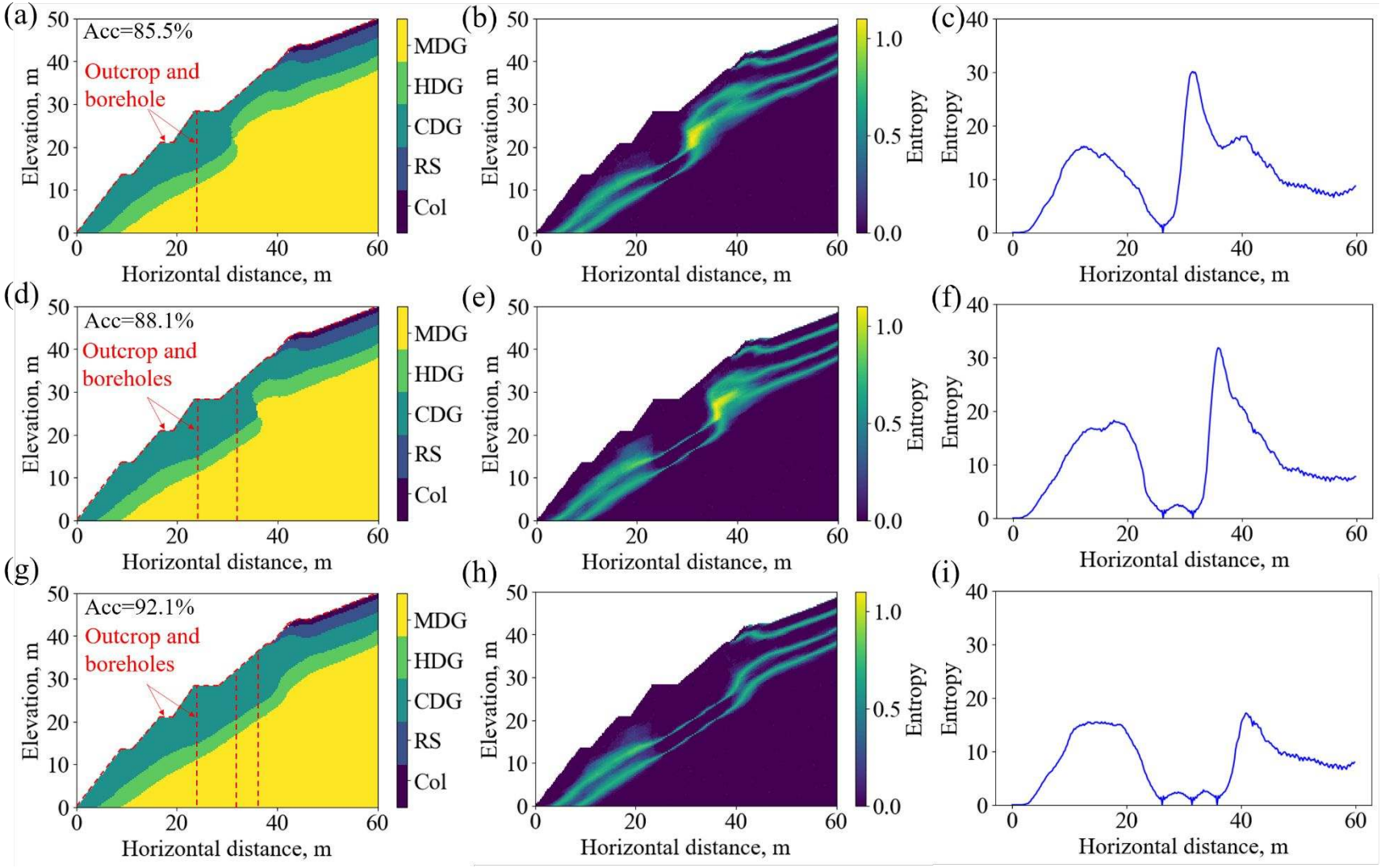

Fig. 19 Evolution of most probable interpolation and information entropy for real slope example: (a) Most probable interpolation (1 borehole); (b) Entropy map (1 borehole); (C) Total entropy curve (1 borehole); (d) Most probable interpolation (2 boreholes); (e) Entropy map (2 boreholes); (f) Total entropy curve (2 boreholes); (g) Most probable interpolation (3 boreholes); (h) Entropy map (3 boreholes); (i) Total entropy curve (3 boreholes)

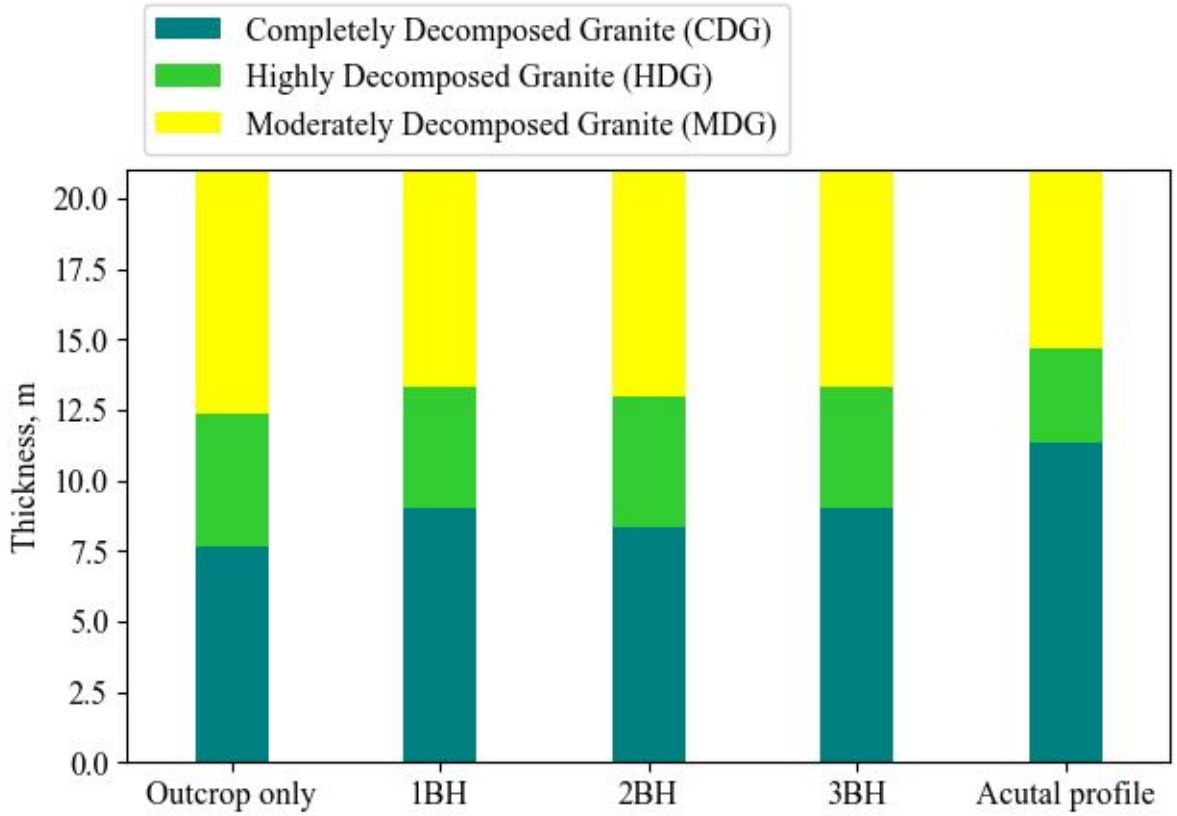

Fig. 20 Comparison of measured and interpolated soil strata along DH4 profile

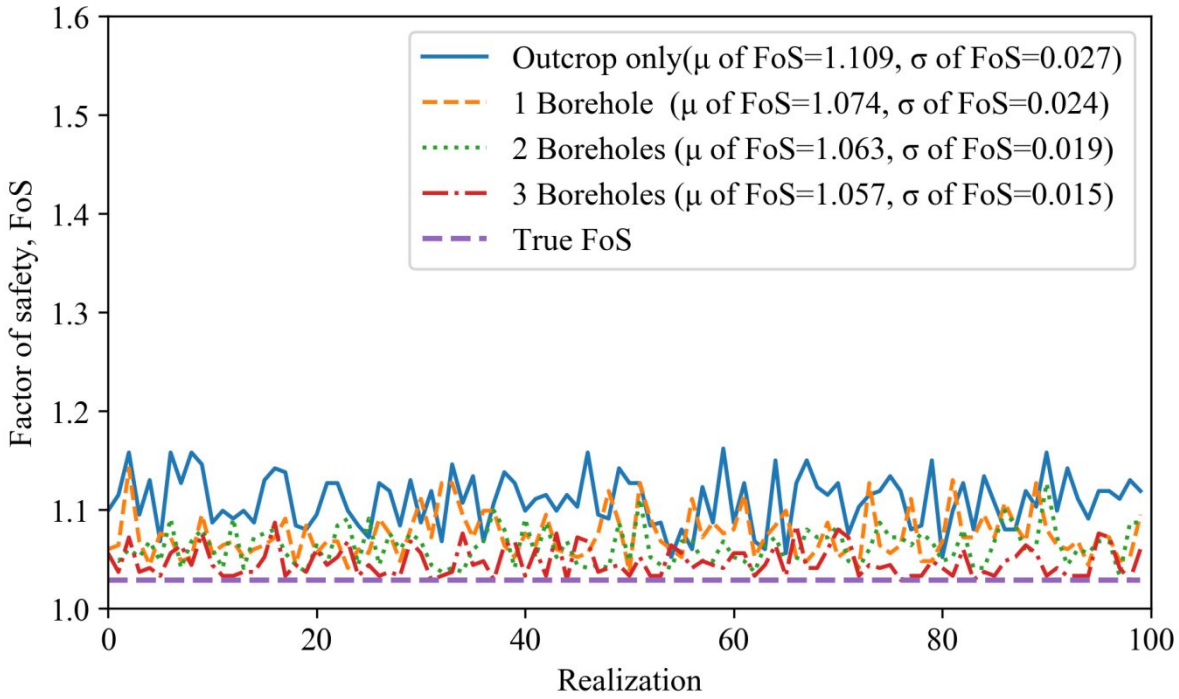

Fig. 21 Evolution of factor of safety with an increasing number of boreholes